

# RANDOMIZED QUASI-OPTIMAL LOCAL APPROXIMATION SPACES IN TIME

JULIA SCHLEUSS, KATHRIN SMETANA, AND LUKAS TER MAAT

**ABSTRACT.** We target time-dependent partial differential equations (PDEs) with coefficients that are arbitrarily rough in both space and time. To tackle these problems, we construct reduced basis/ multiscale ansatz functions defined in space that can be combined with time stepping schemes within model order reduction or multiscale methods. To that end, we propose to perform several simulations of the PDE for few time steps in parallel starting at different, randomly drawn start points, prescribing random initial conditions; applying a singular value decomposition to a subset of the so obtained snapshots yields the reduced basis/ multiscale ansatz functions. This facilitates constructing the reduced basis/ multiscale ansatz functions in an embarrassingly parallel manner. In detail, we suggest using a data-dependent probability distribution based on the data functions of the PDE to select the start points. Each local in time simulation of the PDE with random initial conditions approximates a local approximation space in one time point that is optimal in the sense of Kolmogorov. The derivation of these optimal local approximation spaces which are spanned by the left singular vectors of a compact transfer operator that maps arbitrary initial conditions to the solution of the PDE in a later point of time, is one other main contribution of this paper. By solving the PDE locally in time with random initial conditions, we construct local ansatz spaces in time that converge provably at a quasi-optimal rate and allow for local error control. Numerical experiments demonstrate that the proposed method can outperform existing methods like the proper orthogonal decomposition even in a sequential setting.

## 1. INTRODUCTION

Applications that require repeated simulations for different parameters or a real-time simulation response of complex systems of partial differential equations (PDEs) or dynamical systems are ubiquitous. Moreover, heterogeneous problems that exhibit multiscale features or include rough data functions are particularly challenging. A direct numerical simulation using standard techniques such as the finite element (FE) method can be prohibitively expensive for such tasks. Well-known strategies to tackle these (heterogeneous) problems comprise multiscale methods which are based on local ansatz functions that incorporate the local behavior of the (numerical) solution of the

---

*Date:* March 15, 2022.

*2010 Mathematics Subject Classification.* 65C20, 65M12, 65M15, 65M55, 65M60, 65M75.

*Key words and phrases.* multiscale methods, model order reduction, randomized numerical linear algebra, Kolmogorov n-width.

The work of Julia Schleuß was funded by the Deutsche Forschungsgemeinschaft (DFG, German Research Foundation) under Germany's Excellence Strategy EXC 2044-390685587, Mathematics Münster: Dynamics-Geometry-Structure.

PDE and model order reduction methods that exploit a carefully chosen set of problem-adapted basis functions to reduce the high-dimensional problem. In this paper, we consider time-dependent PDEs and propose reduced basis/ multiscale ansatz functions defined in space that can be combined with time stepping schemes within model order reduction or multiscale methods. To the best of our knowledge, we provide one of the first contributions that facilitates constructing the reduced basis/ multiscale ansatz functions in an embarrassingly parallel manner in time.

A well-established tool for compressing and reducing time trajectories is the proper orthogonal decomposition (POD) [3, 25, 53], which is based on a singular value decomposition (SVD) of the input data matrix and allows for error control. However, in order to perform a POD on simulation data, the (global) solution trajectory of the considered problem has to be computed sequentially prior to reducing.

In contrast, the approach we propose in this paper enables, as one major contribution, to construct reduced basis/ multiscale ansatz functions in parallel in time. To facilitate a time-parallel procedure, we propose to perform several simulations of the PDE for only few time steps in parallel. To this end, we start the simulations at different start time points that are randomly drawn from a data-dependent sampling distribution and prescribe random initial conditions. Subsequently, we apply an SVD to a subset of the computed snapshots to obtain the reduced basis/ multiscale ansatz functions. The proposed method is thus well-suited to be used on modern computer architectures allowing for many parallel computations and on each single compute unit a simulation for only few time steps has to be performed. Moreover, as another major contribution, the approach is especially tailored to time-dependent problems with heterogeneous time-dependent data functions. To draw start time points for the temporally local PDE simulations, we employ uniform, squared norm [18], or leverage score [15] sampling, which are standard sampling techniques from randomized numerical linear algebra (NLA) [10, 14]. In particular, both squared norm and leverage score sampling take into account the time-dependent data functions of the PDE and are commonly used in a variety of applications [10]. While these methods are often used to construct CUR or similar matrix decompositions, we employ them, as one other novel contribution in this paper, for the purpose of time point selection. To this end, the time-dependent data functions are discretized and represented by a matrix, where each column of the matrix corresponds to one time point. Moreover, other randomized subset selection technique, as proposed, for instance, in [1, 12, 11, 13], may also be used to choose time points. We here focus on randomized subset selection techniques as they are often more computationally efficient and robust than deterministic subset selection techniques [10, 14, 21].

The key observation, motivating a localized construction in time, is that for certain time-dependent problems the solution exhibits a very rapid, exponential decay of energy in time. To detect the functions that still persists at a point of time and are thus relevant for approximation, we introduce a compact transfer operator that maps arbitrary initial conditions to the solution of the PDE in a later point of time. Spanning the local space by the leading left singular vectors of the transfer operator results in an approximation space that is optimal in the sense of Kolmogorov [24] and hence minimizes the approximation error among all spaces of the same dimension. While there are many methods that exploit localization in space [2, 20, 33, 32, 38, 39, 40, 54, 16, 22, 23, 30],

we provide with this paper one of the first contributions that exploit localization in time [8, 28].

As a direct calculation of the leading left singular vectors of the transfer operator can become computationally expensive, we employ random sampling as proposed in [5] for elliptic PDEs to efficiently approximate the optimal local spaces and facilitate an embarrassingly parallel construction of the reduced ansatz functions even for a single point of time. To this end, we solve the PDE locally in time with random initial conditions. The resulting local space yields an approximation that converges at a quasi-optimal rate and allows for local error control. While we only provide a local a priori error bound in this paper, we conjecture that it might be possible to also derive a global error bound. Preliminary results can be found in one of the authors bachelor thesis [56], where the proposed method has been tested for problems with time-dependent source terms by uniformly sampling time points.

Optimal spatially local approximation spaces have been introduced for elliptic [2, 29, 54] and parabolic [47] problems, and random sampling has been employed to efficiently approximate the optimal local spaces in the elliptic setting in [5, 7]. Further spatially localizable multiscale methods for parabolic problems have been proposed in [8, 32, 38, 39, 40]. In [28] a space-time multiscale method for the linear heat equation is introduced, where for each coarse space-time node a corrector function that is localized in both space and time is computed to capture (local) fine-scale features. A global a posteriori error bound is proved assuming that certain localization parameters are large enough to guarantee sufficiently small localization errors. Moreover, we refer to [4] for an overview of methods to construct local reduced spaces.

In system and control theory balanced truncation is a well-known method to reduce the complexity of input-output systems [35, 43]. Balanced truncation for systems including time-dependent data functions has been introduced in [51, 59] and its error analysis has been first studied in [26, 45]. Nevertheless, solving matrix differential equations or matrix inequalities is required which is prohibitively expensive for high dimensional problems. In [6] the authors propose an iterative procedure that is computationally more appealing as it is based on operations which exploit sparsity of the model. However, the required computations are global in time and have to be carried out in a sequential manner, leading to a complexity that depends on the global time discretization. In contrast, the approach we propose here requires only local computations in time that are in addition parallelizable.

In [58] it is shown that for linear time-invariant systems the concepts of Kolmogorov  $n$ -widths and Hankel singular values are directly connected and that the right singular vectors of the Hankel operator restricted to the unit ball span the optimal reduced input space in the sense of Kolmogorov and can be linked to active subspaces. We suggest that the leading right singular vectors of the transfer operator introduced here span the optimal reduced input space and can thus be used to regularize inverse problems and data assimilation procedures.

Furthermore, dynamic mode decomposition [48, 57] fits an operator that maps the solution from one time point to the next, and is thus similar to the transfer operator we introduce in this paper, to simulation data. However, similar to the POD and in contrast to the approach we propose here, access to the (global) solution trajectory is required to compress the entire dynamics. Recently, probabilistic numerical methods

that yield a probability distribution over the (unknown) solution of an ordinary or partial differential equation have been proposed, for instance, in [49, 50, 9, 37]. Moreover, randomized subset selection techniques are used in [44] for the purpose of hyperreduction. In comparison, in this paper data-dependent probability distributions and randomized subset selection techniques are exploited to select both start time points and initial conditions for the temporally local PDE simulations.

The remainder of this paper is organized as follows. In [section 2](#) we introduce the general time-dependent model problem together with an exemplary test case and its numerical approximation. Subsequently, we first provide some motivation in [section 3](#) and then develop the main contributions of this paper in [sections 4](#) and [5](#). We propose optimal local spaces in time in [section 4](#) and address their approximation via random sampling in [section 5](#). Moreover, in [section 5](#) we propose a randomized algorithm to construct one reduced space for the global approximation by solving several local problems in time in parallel. We discuss both its basic properties and the choice of the probability distribution used for drawing time points. Finally, we present numerical experiments in [section 6](#) to demonstrate the approximation properties of the proposed algorithm and draw conclusions in [section 7](#).

## 2. PROBLEM SETTING

We consider a time-dependent linear PDE as, for instance, the heat equation or the convection-diffusion equation that may include heterogeneous time-dependent coefficients. To that end, let  $D \subseteq \mathbb{R}^n$  denote a bounded Lipschitz domain of dimension  $n \in \{1, 2, 3\}$  and let  $I = (0, T) \subset \mathbb{R}$  be a time interval with  $0 < T < \infty$ . We assume that on  $I \times D$  a Bochner space  $\mathcal{V}$  and a reflexive Bochner space  $\mathcal{W}$  with dual space  $\mathcal{W}^*$  are given that will serve as ansatz and test space, respectively. Furthermore, we denote by  $\partial_t + \mathcal{A} : \mathcal{V} \rightarrow \mathcal{W}^*$  a linear, continuous, surjective, and inf-sup stable operator. Let  $\mathcal{F} \in \mathcal{W}^*$  be a bounded linear functional. We assume that  $\mathcal{F}$  accounts for both source terms and boundary data. Moreover, we denote the initial values by  $u_0 \in L^2(D)$ . Here, we assume that for any function  $u \in \mathcal{V}$  we have that  $u(t, \cdot) \in L^2(D)$  for every point in time  $t \in I$ . Then, we consider the following variational problem: Find  $u \in \mathcal{V}$  such that  $u(0, \cdot) = u_0$  in  $L^2(D)$  and

$$(2.1) \quad \partial_t u + \mathcal{A}u = \mathcal{F} \quad \text{in } \mathcal{W}^*.$$

The Banach-Nečas-Babuška theorem (e.g. [17, Theorem 2.6]) and the assumptions above guarantee the existence of a unique solution of (2.1).

**Exemplary model problem.** We consider the linear heat equation as a representative model problem of (2.1). To this end, we assume that  $\partial D = \Sigma_D \cup \Sigma_N$  with  $|\Sigma_D| > 0$  and denote by  $f : I \times \Omega \rightarrow \mathbb{R}$  a heat source,  $u_0 : \Omega \times \mathbb{R}$  an initial temperature,  $g_D : I \times \Sigma_D \rightarrow \mathbb{R}$  Dirichlet boundary conditions, and  $g_N : I \times \Sigma_N \rightarrow \mathbb{R}$  Neumann boundary conditions, respectively. In its weak form the heat conductivity coefficient is assumed to satisfy  $\kappa \in L^\infty(I \times D)$  with  $0 < \kappa_0 < \kappa(t, x) < \kappa_1 < \infty$  and  $n$  is the outer unit normal. We then seek the temperature  $u : I \times D \rightarrow \mathbb{R}$  such that

$$(2.2) \quad \begin{aligned} u_t(t, x) - \operatorname{div}(\kappa(t, x) \nabla u(t, x)) &= f(t, x) & \text{for every } (t, x) \in I \times D, \\ u(t, x) &= g_D(t, x) & \text{for every } (t, x) \in I \times \Sigma_D, \\ \kappa(t, x) \nabla u(t, x) \cdot n(x) &= g_N(t, x) & \text{for every } (t, x) \in I \times \Sigma_N, \\ u(0, x) &= u_0(x) & \text{for every } x \in D. \end{aligned}$$

**Discretization.** Here, we consider  $f \in L^2(I, L^2(D))$  and  $g_N \in L^2(I, L^2(\Sigma_N))$ . To simplify notation, we assume that  $f$  also accounts for Dirichlet boundary conditions  $g_D \in L^2(I, H^{1/2}(\Sigma_D))$ . For the numerical approximation of (2.2), we employ the implicit Euler method. To this end, we assume that the time interval  $I$  is partitioned via  $N_I$  equidistant time points  $0 = t_0 < t_1 < \dots < t_{N_I-1} = T$  of distance  $\Delta_T = T/(N_I - 1)$ . However, the approximation can be done completely analogously for other time stepping schemes. Moreover, we consider a piecewise linear conforming FE space  $X$  of dimension  $N_D \in \mathbb{N}$  with basis functions  $\phi_i \in X$ ,  $i = 1, \dots, N_D$ . Then, the mass and stiffness matrices  $\mathbf{M}, \mathbf{A}_l \in \mathbb{R}^{N_D \times N_D}$  and the right-hand side vectors  $\mathbf{F}_l \in \mathbb{R}^{N_D}$  are given as

$$\begin{aligned} \mathbf{M}_{ij} &:= (\phi_j, \phi_i)_{L^2(D)}, \quad 1 \leq i, j \leq N_D, \\ (2.3) \quad (\mathbf{A}_l)_{ij} &:= (\kappa(t_l) \nabla \phi_j, \nabla \phi_i)_{L^2(D)}, \quad 1 \leq i, j \leq N_D, \quad 1 \leq l \leq N_I - 1, \\ (\mathbf{F}_l)_i &:= (f(t_l), \phi_i)_{L^2(D)} + (g_N(t_l), \phi_i)_{L^2(\Sigma_N)}, \quad 1 \leq i \leq N_D, \quad 1 \leq l \leq N_I - 1. \end{aligned}$$

Given a discrete representation  $\mathbf{u}_0 \in \mathbb{R}^{N_D}$  of the initial values  $u_0$ , we approximate the solution of (2.2) by computing  $\mathbf{u}_l \in \mathbb{R}^{N_D}$  at time point  $t_l$  for  $l = 1, \dots, N_I - 1$  via

$$(2.4) \quad (\mathbf{M} + \Delta_T \mathbf{A}_l) \mathbf{u}_l = \Delta_T \mathbf{F}_l + \mathbf{M} \mathbf{u}_{l-1}.$$

**Reduced approximation.** We assume for now that suitable reduced ansatz functions  $\varphi_1, \dots, \varphi_N \in X$  are given that will be determined below (cf. section 5). The matrix  $\mathbf{U}_{\text{red}} = [\varphi_1 \dots \varphi_N] \in \mathbb{R}^{N_D \times N}$  contains the corresponding FE coefficient vectors. We then compute a reduced approximation of (2.4) via Galerkin projection of the FE space onto the space spanned by the reduced basis: For  $l = 1, \dots, N_I - 1$  find  $\mathbf{u}_{\text{red},l} \in \mathbb{R}^N$  such that

$$(2.5) \quad \mathbf{u}_{\text{red},l} = (\mathbf{M}_{\text{red}} + \Delta_T \mathbf{A}_{\text{red},l})^{-1} (\Delta_T \mathbf{F}_{\text{red},l} + \mathbf{M}_{\text{red}} \mathbf{u}_{\text{red},l-1}),$$

where  $\mathbf{M}_{\text{red}} = \mathbf{U}_{\text{red}}^\top \mathbf{M} \mathbf{U}_{\text{red}}$ ,  $\mathbf{A}_{\text{red},l} = \mathbf{U}_{\text{red}}^\top \mathbf{A}_l \mathbf{U}_{\text{red}}$ ,  $\mathbf{F}_{\text{red},l} = \mathbf{U}_{\text{red}}^\top \mathbf{F}_l$ , and  $\mathbf{u}_{\text{red},0} = \mathbf{M}_{\text{red}}^{-1} \mathbf{U}_{\text{red}}^\top \mathbf{M} \mathbf{u}_0$ .

### 3. MOTIVATION

To construct reduced ansatz functions  $\varphi_1, \dots, \varphi_N \in X$  as given above, a well-established strategy is to perform a POD on (the first part of) the global solution trajectory. For this purpose, prior to reducing, the global solution in time has to be computed in a sequential manner. In contrast, the method we propose in this paper generates a reduced basis in an embarrassingly time-parallel manner by drawing time points from a data-dependent sampling distribution as indicated in Fig. 1. Subsequently, reduced ansatz functions corresponding to the selected time points are generated in parallel by solving independent local problems in time. Consequently, the proposed approach enables to split and distribute the computational budget over the entire time interval and is thus well-suited to be used on modern computer architectures allowing for many parallel computations.

To motivate a localized construction of the reduced ansatz functions in time, we recall the following well-known property that many time-dependent problems share via the example of the linear heat equation: If  $\mathcal{F} \equiv 0$  it is straightforward to show that  $\|u(t, \cdot)\|_{L^2(D)} \leq e^{-Ct} \|u_0\|_{L^2(D)}$  for any  $t \in I$ , where the constant  $C$  depends only on the shape of  $D$  and the heat conductivity coefficient. To detect the functions that still persist at a selected time point  $t$  and are thus relevant for approximation purposes, we introduce a transfer operator  $\mathcal{T}_{s \rightarrow t}$  that takes arbitrary initial conditions in  $L^2(D)$  at

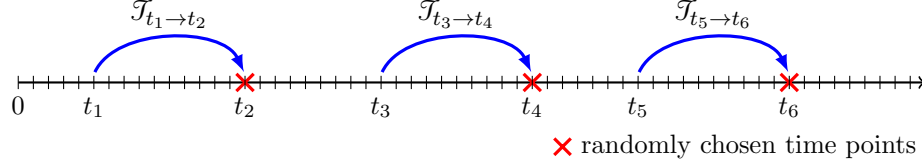


FIGURE 1. Transfer operators corresponding to randomly chosen time points.

time  $s \in I$  with  $s < t$ , solves the PDE locally in  $(s, t)$ , and evaluates the solution at target time  $t$ ; see Fig. 1 for an illustration. In this way, the transfer operator captures the decay behavior of solutions of the PDE in time.

After discretization, say, with the FE method, the transfer operator can be represented by a matrix. According to the well-known Eckart-Young theorem the range of this matrix can be optimally approximated by its leading left singular vectors. While the *discrete* transfer operator is trivially compact thanks to its finite rank, in the *continuous* setting we need to prove compactness of the transfer operator to facilitate its singular value decomposition (SVD) via the Hilbert-Schmidt theorem [42, Theorem 8.94]. Then, the space spanned by the leading left singular vectors provides an optimal approximation in the sense of Kolmogorov, meaning that it minimizes the approximation error among all linear spaces of the same dimension (see [41, Theorem 2.2 in Chapter 4]).

To further facilitate an efficient parallel computation, we approximate the optimal spaces via random sampling [5, 21], i.e. we solve the PDE locally in time with random initial conditions, which results in a provably nearly optimal local approximation.

#### 4. OPTIMAL LOCAL APPROXIMATION SPACES IN TIME

In this section we propose local approximation spaces in time, which are optimal in the sense of Kolmogorov for the approximation of the solution of (2.1) in a point of time  $t$ . The coefficients may be rough in both space and time. We address the construction of the optimal local ansatz spaces in time in subsection 4.1. Subsequently, we show how to compute an approximation of the optimal local spaces and discuss its practical realization via Krylov subspace methods and random sampling in subsection 4.2.

**4.1. Constructing optimal local approximation spaces via a transfer operator.** We first observe that for any local subinterval  $(s, t) \subseteq I$  of the global time interval the solution  $u$  of (2.1) solves the PDE locally in time with (unknown) initial conditions given by  $u(s, \cdot) \in L^2(D)$ . Therefore, we consider all local solutions  $u_{\text{loc}} \in \mathcal{V}|_{(s,t) \times D}$  with arbitrary initial conditions  $u_{\text{loc}}(s, \cdot) \in L^2(D)$  that satisfy

$$(4.1) \quad \partial_t u_{\text{loc}} + \mathcal{A}_{\text{loc}} u_{\text{loc}} = \mathcal{F}_{\text{loc}} \quad \text{in } (\mathcal{W}|_{(s,t) \times D})^*.$$

Here,  $\mathcal{A}_{\text{loc}}$  and  $\mathcal{F}_{\text{loc}}$  denote the respective local operator and functional associated with  $(s, t) \times D$ . All solutions of (4.1) can be split into a function that solves (4.1) for  $\mathcal{F}_{\text{loc}}$  and homogeneous initial conditions and a function that solves (4.1) for  $\mathcal{F}_{\text{loc}} \equiv 0$  and arbitrary initial conditions. In the following, we will first address the case where  $\mathcal{F}_{\text{loc}} \equiv 0$  and discuss the general case at the end of the subsection.

As we want to approximate the evaluation of the global solution at time point  $t$ , we consider the space  $\mathcal{H}_t$  of all solutions of (4.1) evaluated at time  $t$ :

$$(4.2) \quad \mathcal{H}_t := \{w(t, \cdot) \in L^2(D) \mid w \in \mathcal{V}|_{(s,t) \times D} \text{ solves (4.1), } w(s, \cdot) \in L^2(D), \mathcal{F}_{\text{loc}} \equiv 0\}.$$

We equip the space  $\mathcal{H}_t$  with the  $L^2(D)$ -inner product and -norm. To approximate the local solution space at time  $t$ , we then define a transfer operator  $\mathcal{T}_{s \rightarrow t} : L^2(D) \rightarrow \mathcal{H}_t$  for  $s < t$ ,  $s \in I$ , that is given by

$$(4.3) \quad \mathcal{T}_{s \rightarrow t} w(s, \cdot) = w(t, \cdot) \quad \text{for } w \in \mathcal{V}|_{(s,t) \times D} \text{ and thus } w(s, \cdot) \in L^2(D).$$

**Assumption 1.** *We assume that the transfer operator  $\mathcal{T}_{s \rightarrow t}$  introduced in (4.3) is compact for arbitrary  $0 \leq s < t \leq T$ .*

Compactness of the transfer operator guarantees the existence of its SVD via the Hilbert-Schmidt theorem [42, Theorem 8.94]. Similar to [2, 47, 54] it can then be shown that the leading left singular vectors of  $\mathcal{T}_{s \rightarrow t}$  span an optimal approximation space in the local solution space  $\mathcal{H}_t$ . Here, we use the concept of optimality in the sense of Kolmogorov [24]: A subspace  $\mathcal{H}_t^n \subset \mathcal{H}_t$  of dimension at most  $n$  for which holds  $d_n(\mathcal{T}_{s \rightarrow t}(\mathcal{H}_s); \mathcal{H}_t) = \|\mathcal{T}_{s \rightarrow t} - \mathcal{P}_{\mathcal{H}_t^n} \mathcal{T}_{s \rightarrow t}\|$  is called an optimal subspace for  $d_n(\mathcal{T}_{s \rightarrow t}(\mathcal{H}_s); \mathcal{H}_t)$ , where the Kolmogorov  $n$ -width  $d_n(\mathcal{T}_{s \rightarrow t}(\mathcal{H}_s); \mathcal{H}_t)$  is defined as  $d_n(\mathcal{T}_{s \rightarrow t}(\mathcal{H}_s); \mathcal{H}_t) := \inf_{\mathcal{H}_t^n \subset \mathcal{H}_t; \dim(\mathcal{H}_t^n) = n} \|\mathcal{T}_{s \rightarrow t} - \mathcal{P}_{\mathcal{H}_t^n} \mathcal{T}_{s \rightarrow t}\|$  and  $\mathcal{P}_{\mathcal{H}_t^n}$  denotes the orthogonal projection onto  $\mathcal{H}_t^n$ .

**Theorem 4.1** (Optimal local approximation spaces in time). *Let  $\sigma_{s \rightarrow t}^{(i)} \in \mathbb{R}^+$  and  $\varphi_{s \rightarrow t}^{(i)} \in \mathcal{H}_t$ ,  $i = 1, \dots, \infty$ , denote the singular values and left singular vectors of the transfer operator  $\mathcal{T}_{s \rightarrow t}$  defined in (4.3). Then the optimal approximation space for  $d_n(\mathcal{T}_{s \rightarrow t}(\mathcal{H}_s); \mathcal{H}_t)$  is given by*

$$(4.4) \quad \mathcal{H}_t^n := \text{span}\{\varphi_{s \rightarrow t}^{(1)}, \dots, \varphi_{s \rightarrow t}^{(n)}\}$$

and the Kolmogorov  $n$ -width satisfies

$$d_n(\mathcal{T}_{s \rightarrow t}(\mathcal{H}_s); \mathcal{H}_t) = \sup_{\psi \in \mathcal{H}_s} \inf_{\zeta \in \mathcal{H}_t^n} \frac{\|\mathcal{T}_{s \rightarrow t} \psi - \zeta\|_{L^2(D)}}{\|\psi\|_{L^2(D)}} = \|\mathcal{T}_{s \rightarrow t} - \mathcal{P}_{\mathcal{H}_t^n} \mathcal{T}_{s \rightarrow t}\| = \sigma_{s \rightarrow t}^{(n+1)}.$$

*Proof.* The assertion directly follows from the Hilbert-Schmidt theorem [42, Theorem 8.94] and [41, Theorem 2.2 in Chapter 4].  $\square$

To address non-homogeneous data  $\mathcal{F}_{\text{loc}}$ , we define  $u_{s \rightarrow t}^f \in \mathcal{V}|_{(s,t) \times D}$  as the solution of (4.1) with homogeneous initial conditions at time  $s$ . Finally, the optimal local approximation space at time  $t$  is given by

$$(4.5) \quad \mathcal{H}_t^{n, \text{data}} := \text{span}\{\varphi_{s \rightarrow t}^{(1)}, \dots, \varphi_{s \rightarrow t}^{(n)}, \varphi_{s \rightarrow t}^f\}, \quad \varphi_{s \rightarrow t}^f := u_{s \rightarrow t}^f(t, \cdot) - \mathcal{P}_{\mathcal{H}_t^n} u_{s \rightarrow t}^f(t, \cdot).$$

**Remark 4.2.** In Appendix A we consider the linear heat equation as an exemplary model problem of (2.1) and exemplarily prove compactness of the corresponding transfer operator.

**4.2. Approximation of the optimal local approximation spaces in time.** In this subsection we describe how to compute an approximation of the optimal local space  $\mathcal{H}_t^{n, \text{data}}$  in (4.5) for the example of the linear heat equation (cf. section 2). In the following, we use the notation introduced in section 2 (see e.g. (2.3)). Assuming that  $s = t_i$  and  $t = t_j$  for  $0 \leq i < j \leq N_I - 1$  and given a discrete version  $\mathbf{u}_{\text{loc}, i} \in \mathbb{R}^{N_D}$  of the arbitrary local initial values  $u_{\text{loc}}(s, \cdot)$ , we compute a local solution  $\mathbf{u}_{\text{loc}, l} \in \mathbb{R}^{N_D}$  at time point  $t_l$  for  $l = i + 1, \dots, j$  via (cf. (2.4) and (4.1))

$$(4.6) \quad \mathbf{u}_{\text{loc}, l} = (\mathbf{M} + \Delta_T \mathbf{A}_l)^{-1} (\Delta_T \mathbf{F}_l + \mathbf{M} \mathbf{u}_{\text{loc}, l-1}).$$



As the discrete transfer operator  $T_{t_i \rightarrow t_j}$  acts on the space of local solutions with  $\mathbf{F}_l = 0$  ( $i \leq l \leq j$ ), the matrix version  $\mathbf{T}_{t_i \rightarrow t_j} \in \mathbb{R}^{N_D \times N_D}$  of  $T_{t_i \rightarrow t_j}$  is given by (cf. (4.3))

$$(4.7) \quad \mathbf{T}_{t_i \rightarrow t_j} \boldsymbol{\xi} = [(\mathbf{M} + \Delta_T \mathbf{A}_j)^{-1} \mathbf{M}] [(\mathbf{M} + \Delta_T \mathbf{A}_{j-1})^{-1} \mathbf{M}] \dots [(\mathbf{M} + \Delta_T \mathbf{A}_{i+1})^{-1} \mathbf{M}] \boldsymbol{\xi}.$$

Finally, we compute the  $n$  leading left singular vectors  $\varphi_{t_i \rightarrow t_j}^{(1)}, \dots, \varphi_{t_i \rightarrow t_j}^{(n)} \in \mathbb{R}^{N_D}$  of  $\mathbf{T}_{t_i \rightarrow t_j}$  to approximate the optimal local space  $\mathcal{H}_{t_j}^n$  (cf. (4.4)) and define

$$(4.8) \quad H_{t_j}^n := \text{span}\{\varphi_{t_i \rightarrow t_j}^{(1)}, \dots, \varphi_{t_i \rightarrow t_j}^{(n)}\},$$

where  $\varphi_{t_i \rightarrow t_j}^{(k)}$  is the FE function corresponding to the coefficient vector  $\varphi_{t_i \rightarrow t_j}^{(k)}$  for  $1 \leq k \leq n$ . Consequently, we have that  $\|T_{t_i \rightarrow t_j} - P_{H_{t_j}^n} T_{t_i \rightarrow t_j}\| = \sigma_{t_i \rightarrow t_j}^{(n+1)}$  (Eckart-Young theorem e.g. in [19]), where  $\sigma_{t_i \rightarrow t_j}^{(n+1)}$  is the  $n+1$ -st singular value of  $T_{t_i \rightarrow t_j}$  (listed in non-increasing order of magnitude) and  $P_{H_{t_j}^n}$  denotes the orthogonal projection onto  $H_{t_j}^n$  (cf. Theorem 4.1). We use the same notation for continuous and discrete singular values and vectors expecting that the respective meaning is clear from the context.

To address non-homogeneous data  $\mathbf{F}_l$  ( $l = i+1, \dots, j$ ), we compute the solution of (4.6) for homogeneous initial conditions  $\mathbf{u}_{\text{loc},i}^{\mathbf{F}} \equiv 0$ , add the resulting solution  $\mathbf{u}_{\text{loc},j}^{\mathbf{F}}$  at time  $t_j$  to the FE basis, and define  $H_{t_j}^{n,\text{data}}$  as the span of the FE functions associated with the coefficient vectors  $\varphi_{t_i \rightarrow t_j}^{(1)}, \dots, \varphi_{t_i \rightarrow t_j}^{(n)}, \mathbf{u}_{\text{loc},j}^{\mathbf{F}}$ .

**Remark 4.3** (Comparison of computational approaches to approximate the optimal local spaces). *In practice, the left singular vectors of  $\mathbf{T}_{t_i \rightarrow t_j}$  can be computed via the eigenvectors of  $\mathbf{T}_{t_i \rightarrow t_j}^\top \mathbf{T}_{t_i \rightarrow t_j}$ . A direct computation of the optimal local space would therefore require to compute the evaluation of local solutions at time  $t_j$  for all  $N_D$  basis functions that span the local solution space at time  $t_i$ , thus evaluate the transfer operator  $N_D$  times, and solve a dense generalized eigenproblem of dimension  $N_D \times N_D$ . As this becomes infeasible for large  $N_D$ , one would in general use Krylov subspace or randomized methods for the approximation of the optimal local spaces [5, 21, 34].*

*In Krylov subspace methods, the application of the transfer operator (4.7) would be implicitly passed to the eigenvalue solver. To calculate the  $m$  leading eigenvectors of  $\mathbf{T}_{t_i \rightarrow t_j}^\top \mathbf{T}_{t_i \rightarrow t_j}$  using, for instance, the implicitly restarted Arnoldi method (IRAM) from [27],  $\mathcal{O}(m)$  evaluations of  $\mathbf{T}_{t_i \rightarrow t_j}$  and  $\mathbf{T}_{t_i \rightarrow t_j}^\top$  are required in every iteration. While Krylov subspace methods can lead to more accurate approximations especially for slowly decaying singular values, randomized methods have the main advantage that they are inherently stable and amenable to parallelization [21, 60].*

*To approximate the space spanned by the  $m$  leading left singular vectors of the transfer operator via random sampling as described in subsection 5.1 in more detail,  $m+s$  evaluations of the transfer operator are required. As randomized methods can outperform Krylov subspace methods even in the sequential setting (see, e.g., [5]), they are thus an appealing choice for the approximation of the optimal local spaces. For a more in-depth comparison of Krylov subspace and randomized methods, we refer, for instance, to [21, section 6].*

**Remark 4.4** (Computational complexity). *The computational complexity of the local basis construction is clearly dominated by the evaluation of  $\mathbf{T}_{t_i \rightarrow t_j}$  or  $\mathbf{T}_{t_i \rightarrow t_j}^\top$  and thus the numerical solution of the local PDE, where we employ a sparse direct solver. For a standard FE discretization in two or three dimensions the factorizations of  $(\mathbf{M} +$*



$\Delta_T \mathbf{A}_{i+1}, \dots, (\mathbf{M} + \Delta_T \mathbf{A}_j) \in \mathbb{R}^{N_D \times N_D}$  can be computed in  $\mathcal{O}((j-i)N_D^{3/2})$  or  $\mathcal{O}((j-i)N_D^2)$  work [19]. After factorizing, the computational complexity for each local solution trajectory of the PDE is  $\mathcal{O}((j-i)N_D \log(N_D))$  or  $\mathcal{O}((j-i)N_D^{4/3})$  [19].

## 5. QUASI-OPTIMAL LOCAL APPROXIMATION SPACES IN TIME VIA RANDOM SAMPLING

In this section we show how we can exploit techniques from randomized NLA [5, 15, 18, 10, 14, 21] to derive a randomized algorithm that provides an approximation to the (discrete) solution of problem (2.1) (see also motivation in section 3). For this purpose, the proposed algorithm randomly chooses time points based on a probability distribution that accounts for the time-dependent data functions of the problem. While the space  $H_{t_j}^n$  (cf. (4.8)) provides an optimal approximation for the local solution space in each selected time point  $t_j$ , we employ random sampling [5] to generate ansatz functions with provably nearly optimal approximation properties in an efficient and embarrassingly parallel manner. To this end, the transfer operator  $T_{t_i \rightarrow t_j}$  (cf. (4.7)) is applied to random initial conditions, i.e. the PDE is solved on the interval  $(t_i, t_j)$  with random initial conditions prescribed at time  $t_i$  and the resulting local solution is evaluated at time  $t_j$ . Having solved all local problems for the selected time points, we finally compress the local ansatz functions to construct one reduced space in time to approximate the (discrete) solution of the global problem (2.1).

The proposed algorithm thus enables to split and distribute the available computational budget over the entire time interval and only requires the solution of local PDEs on small time intervals. All local PDEs can be solved independently from each other and consequently its computation is embarrassingly parallel. The proposed algorithm is thus well-suited to be used on modern computer architectures. Moreover, the proposed approach allows for local error control. Employing the adaptive randomized range finder algorithm from [5], we can adaptively construct a reduced basis that satisfies a prescribed local error tolerance in each chosen time point.

In this section we abuse notation and denote by  $H_{t_j}^n$  and  $T_{t_i \rightarrow t_j}$  (cf. subsection 4.2) the discrete optimal local space and transfer operator associated with a general model problem (2.1). We emphasize that the results are not restricted to the exemplary case of the linear heat equation.

In subsection 5.1, we first sketch how one optimal space  $H_{t_j}^n$  for a time point  $t_j \in I$  can be approximated via random sampling. In subsection 5.2, we then present the randomized algorithm for the approximation of the global solution of (2.1) and discuss its basic properties. Subsequently, we address the choice of the probability distribution that is used to draw time points in subsection 5.3.

### 5.1. Approximating the range of one transfer operator via random sampling.

To construct a suitable approximation  $H_{t_j, \text{rand}}^n$  of the optimal local space  $H_{t_j}^n$  (cf. (4.8)), we prescribe  $n = m + s$  random initial conditions at the local starting time  $t_i < t_j$ , where the coefficient vectors of the corresponding FE functions are mutually independent standard normal random vectors  $\mathbf{r}_1, \dots, \mathbf{r}_n \sim N(\mathbf{0}, (\mathbf{A}_i^\top \mathbf{A}_i)^{-1})$ . Recall that  $\mathbf{A}_i$  denotes the stiffness matrix corresponding to time point  $t_i$  (cf. (2.3)). Then, the matrix version of the transfer operator  $\mathbf{T}_{t_i \rightarrow t_j}$  (cf. (4.7)) is applied to the random vectors, meaning we solve the PDE locally on the time interval  $(t_i, t_j)$  with initial conditions given by  $\mathbf{r}_1, \dots, \mathbf{r}_n$  and evaluate the solutions at the local end time  $t_j$ . Here, the computation

of the  $n$  local solutions is embarrassingly parallel. The space  $H_{t_j, \text{rand}}^n$  is then spanned by the  $n$  resulting local solutions evaluated at time  $t_j$ .

The following probabilistic a priori error bound shows that the space  $H_{t_j, \text{rand}}^n$  yields an approximation that converges at a nearly optimal rate which is only slightly worse than the rate  $\sigma_{t_i \rightarrow t_j}^{(n+1)}$  achieved by the optimal space  $H_{t_j}^n$  (cf. [subsection 4.2](#)).

**Proposition 5.1.** (Probabilistic a priori error bound, [\[5, Proposition 3.2\]](#) based on [\[21, Theorem 10.6\]](#)). *Let  $\lambda_{\min}^{\mathbf{M}}$  and  $\lambda_{\max}^{\mathbf{M}}$  denote the smallest and largest eigenvalue of  $\mathbf{M}$  (cf. [\(2.3\)](#)). Moreover, we denote by  $\sigma_{\min}^{\mathbf{A}_i}$  and  $\sigma_{\max}^{\mathbf{A}_i}$  the smallest and largest singular value of  $\mathbf{A}_i$ . Then, for  $n \geq 4$  it holds that*

$$(5.1) \quad \mathbb{E}(\|T_{t_i \rightarrow t_j} - P_{H_{t_j, \text{rand}}^n} T_{t_i \rightarrow t_j}\|) \leq \frac{\sigma_{\max}^{\mathbf{A}_i} \lambda_{\max}^{\mathbf{M}}}{\sigma_{\min}^{\mathbf{A}_i} \lambda_{\min}^{\mathbf{M}}} \min_{\substack{m+s=n \\ m \geq 2, s \geq 2}} \left[ \left(1 + \left(\frac{m}{s-1}\right)^{1/2}\right) \sigma_{t_i \rightarrow t_j}^{(m+1)} + \frac{e\sqrt{n}}{s} \left(\sum_{l>m} (\sigma_{t_i \rightarrow t_j}^{(l)})^2\right)^{1/2} \right].$$

*Proof.* By applying the Courant minimax principle the result follows directly from [\[5, Proposition 3.2\]](#), which is based on [\[21, Theorem 10.6\]](#).  $\square$

As we can hope that the transfer operator has a fast decaying spectrum, the square root of the sum of squared singular values in the last term of [\(5.1\)](#) behaves often roughly as  $\sigma_{t_i \rightarrow t_j}^{(m+1)}$ . For further details we refer to [\[5\]](#) where methods from randomized linear algebra [\[21\]](#) have been used to approximate the optimal local approximation spaces in the elliptic setting.

**5.2. Fixed-number of initial conditions algorithm.** As introduced in [section 2](#), we assume that the time interval  $I$  is discretized via  $N_I \in \mathbb{N}$  time points  $0 = t_0 \leq \dots \leq t_{N_I-1} = T$ . To provide a good approximation of the (discrete) solution of problem [\(2.1\)](#), we propose to randomly choose a subset of time points in  $\{t_0, \dots, t_{N_I-1}\}$  according to a probability distribution that may reflect the time-dependent data functions of the considered problem (cf. [subsection 5.3](#)). To construct suitable ansatz functions in the chosen time points, we then apply the corresponding transfer operators to random initial conditions (cf. [subsection 5.1](#)) as depicted in [Fig. 2](#). Here, the local PDEs are solved for  $n_t$  time steps. Subsequently, we store the local solution trajectories evaluated at the locally last (randomly chosen) time points. By tuning the parameter  $k$ , we decide to additionally store the local solutions evaluated at local time points  $k, k+1, \dots, n_t-1$ . In this way, we sample from the ranges of multiple transfer operators simultaneously and possibly incorporate additional modes that are relevant for approximation purposes. Finally, we compress all stored local ansatz functions via an SVD to construct the (time-dependent) reduced approximation space.

[Algorithm 1](#) summarizes the randomized basis generation. In detail, in [line 2](#) we first draw  $n_{\text{rand}} \in \mathbb{N}$  integers in the set  $\{0, \dots, N_I-1\}$  that correspond to  $n_{\text{rand}}$  time points in  $\{t_0, \dots, t_{N_I-1}\}$  using the probability distribution  $p$ . The choice of  $n_{\text{rand}}$  can be based, for instance, on the number of parallel compute units provided by the employed computer architecture. In addition, it should be guided by the rank of the time-dependent data functions of the considered problem in order to ensure a good approximation quality with high probability (cf. the experiments in [section 6](#)). Depending on the particular model problem, one might either sample solely from one probability distribution or sample simultaneously from two (or more) distributions, each corresponding

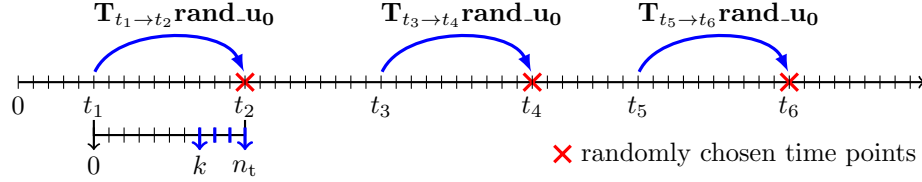


FIGURE 2. Evaluation of multiple transfer operators at randomly chosen points in time for random initial conditions. Sketch of parameters  $k$  and  $n_t$  in Algorithm 1.

to one data function of the considered problem. In the following we assume that the probability distribution  $p$  is given and refer to subsection 5.3 for details on the choice of  $p$  and how to sample from multiple distributions.

The time points chosen according to  $p$  indicate the end time points for the temporally local solutions of the PDE (evaluations of the transfer operators) and automatically determine the corresponding start time points. As the oversampling parameter  $n_t (\ll N_I)$  specifies the number of time steps used for computing the local solutions, we check in line 3 if any of the chosen integers is smaller than or equal to  $n_t$ . In this case, we remove the respective entry from the set of chosen integers in line 4. All time points smaller than or equal to  $t_{n_t}$  are included in the computations in line 11, where we compute the evolution of the initial conditions  $\mathbf{u}_0$  for the first  $n_t$  time steps. In line 5 we then assign the lists of start and end time points for the temporally local solutions of the PDE (evaluations of the transfer operators), where the local start time points are given by the chosen end time points minus  $n_t$  time steps.

Subsequently, in line 6 we initialize the snapshot matrix  $\mathbf{S}$  that is used for collecting the random local solutions evaluated at certain points in time (snapshots). Next, for each starting point in time, we first draw in line 8 a Gaussian random vector  $\mathbf{rand.u}_0$  that will serve as the local initial condition. One possibility is to choose  $\mathbf{rand.u}_0 \sim N(\mathbf{0}, (\mathbf{A}_i^\top \mathbf{A}_i)^{-1})$ , where  $\mathbf{A}_i$  is the stiffness matrix corresponding to the (local start) time point  $t_i$  (cf. (2.3) and subsection 5.1).

In line 9, we then compute the local solution of the PDE with initial condition  $\mathbf{rand.u}_0$  for the local time interval given by the respective random start and end time points. For this purpose, we employ the suitably chosen (with respect to the particular PDE) time stepping scheme  $\mathbf{t\_steps}$  that is given as an input by the user. Finally, we store the resulting local solution evaluated at the last  $n_t - k + 1$  ( $k \leq n_t$ ) time points in the matrix **snapshots** and add it to the snapshot matrix  $\mathbf{S}$  in line 10. By choosing the parameter  $k$  smaller than  $n_t$ , we sample from the range of multiple transfer operators simultaneously. As the numerical experiments in section 6 show, collecting solution snapshots for more than the last time instance often results in an improved approximation accuracy.

Based on the findings in section 6, we propose  $k = n_t - 2$  as a reasonable choice for diffusion problems, while for advection-dominated problems a smaller  $k$ , say,  $k = n_t - 5$ , might be more favorable. An appropriate choice for  $n_t$  seems to be 10 – 15, while for  $n_t = 10$  the resulting reduced basis is larger compared to  $n_{\text{rand}} = 15$  and the user can balance computational costs depending on the respective application.

For transfer operators with a fast decaying spectrum we observe in the numerical experiments that it is sufficient to draw only one random initial condition and thus compute only one local basis function per chosen time point as proposed in lines 8-9. We

**Algorithm 1:** Reduced basis generation via random sampling and SVD

---

```

1 Function RandomizedReducedBasisGeneration( $n_{\text{rand}}, n_t, k, p, \text{tol}$ ):
    Input :  $n_{\text{rand}}, n_t, k (\leq n_t), p, \text{t\_steps}, \text{tol}$ 
    Output: reduced basis  $\mathbf{U}_{\text{red}}$  chosen according to tolerance  $\text{tol}$ 
2   rand_ints  $\leftarrow$  draw  $n_{\text{rand}}$  integers in  $\{0, \dots, N_I - 1\}$  according to  $p$ 
3   if rand_ints[i]  $\leq n_t$  then
4     | remove entry rand_ints[i] from rand_ints
5   endpoints  $\leftarrow$  timegrid[rand_ints], startpoints  $\leftarrow$  timegrid[rand_ints -  $n_t$ ]
6    $\mathbf{S} \leftarrow \emptyset$ 
7   for  $i = 1, \dots, \#\text{startpoints}$  do
8     | // draw random initial condition
9     | rand_u0  $\leftarrow$  Gaussian(size =  $N_D$ )
10    | // solve locally and store solution at time steps  $k$  to  $n_t$ 
11    | snapshots  $\leftarrow$  t_steps(startpoints[i], endpoints[i],  $n_t$ , rand_u0)[ $:, k : n_t$ ]
12    |  $\mathbf{S} \leftarrow [\mathbf{S}, \text{snapshots}]$ 
13  | // add representation of  $\mathbf{u}_0$  for first  $n_t$  time steps
14  | snapshots_u0  $\leftarrow$  t_steps(0, timegrid[ $n_t$ ],  $n_t$ ,  $\mathbf{u}_0$ )
15  |  $\mathbf{S} \leftarrow [\mathbf{S}, \text{snapshots\_u0}]$ 
16  | // compute SVD of collected snapshots and cut using tol
17  |  $\mathbf{U}_{\text{red}}, -, - \leftarrow \text{svd}(\mathbf{S}, \text{tol})$ 

```

---

therefore do not split the computation in line 9 into solving for random initial conditions and homogeneous right-hand side and solving for homogeneous initial conditions and right-hand side. However, as discussed in Remark 5.2, for problems where the spectra of the transfer operators decay more slowly, we suggest to draw multiple random initial conditions and thus compute multiple local basis functions per chosen time point in order to improve the accuracy of the approximation.

As indicated above, we compute the evolution of the initial conditions  $\mathbf{u}_0$  for the first  $n_t$  time steps in line 11 and add it to the snapshot matrix  $\mathbf{S}$  in line 12. We highlight that the computations in lines 7 to 11 are embarrassingly parallel.

Having collected all snapshots, we finally compute an SVD of the snapshot matrix  $\mathbf{S}$  in line 13 to extract the most significant modes. To this end, we calculate the value of  $c_i := (\sum_{j=i+1}^{n_s} \sigma_j^2 / \sum_{j=1}^{n_s} \sigma_j^2)^{1/2}$  for  $i = 1, 2, \dots$ , where  $\sigma_1, \dots, \sigma_{n_s}$  denote the singular values of  $\mathbf{S}$ . The smallest integer  $i^*$  that meets the condition  $c_{i^*} \leq \text{tol}$ , where the tolerance  $\text{tol}$  is chosen by the user, determines the size of the reduced basis  $\mathbf{U}_{\text{red}}$ . The latter contains the leading  $i^*$  left singular vectors of  $\mathbf{S}$  and is returned as the output of Algorithm 1.

**Remark 5.2** (Number of random initial conditions per time point). *In lines 8-9 of Algorithm 1 we propose to draw one random initial condition and thus compute one local basis function per chosen time point. In light of the probabilistic a priori error bound (5.1) and the quasi-optimal convergence rate obtained by the randomized approximations, we conjecture that for transfer operators with a fast decaying spectrum this is sufficient in order to obtain a good approximation accuracy and also observe this in the numerical experiments at least for the considered test cases.*

However, for transfer operators with a more slowly decaying spectrum, induced by, say, rapidly varying heterogeneous time-dependent data functions, we suggest to draw multiple random initial conditions per chosen time point to enhance the quality of the approximation. In that case, the computation in line 9 has to be splitted into (multiply) solving for random initial conditions and homogeneous right-hand side and (once) solving for homogeneous initial conditions and right-hand side.

Employing the adaptive randomized range finder algorithm from [5], the number of initial conditions in each time point can be determined adaptively. To this end, the user prescribes a desired local error tolerance and, based on a probabilistic a posteriori error estimator, the local reduced basis is adaptively enhanced with evaluations of the transfer operator for random initial conditions until the tolerance is satisfied.

**Remark 5.3** (Computational complexity of Algorithm 1). Assuming that we employ the discretization introduced in section 2 and subsection 4.2, the complexity for computing the  $n_{\text{rand}} + 1$  solution trajectories in lines 9 and 11 of Algorithm 1 is  $\mathcal{O}((n_{\text{rand}} + 1)n_t(N_D^{3/2} + N_D \log(N_D)))$  in two or  $\mathcal{O}((n_{\text{rand}} + 1)n_t(N_D^2 + N_D^{4/3}))$  in three spatial dimensions (cf. Remark 4.4). We highlight that the computations in lines 9 and 11 are embarrassingly parallel as the local solution trajectories can be computed completely independently from each other. Algorithm 1 is thus well-suited to be used on modern computer architectures allowing for many parallel computations.

Moreover, the computational complexity for compressing the collected snapshots via an SVD in line 13 is  $\mathcal{O}((n_t - k + 1)n_{\text{rand}} + n_t)N_D^2$ . Alternatively, we can approximate the SVD of  $\mathbf{S}$  via a randomized SVD [21]. For details on the computational complexity of assembling the probability distribution  $p$  we refer to subsection 5.3.

**Remark 5.4** (Choice of  $n_{\text{rand}}$ ). In Algorithm 1 the user determines the number of random initial conditions  $n_{\text{rand}}$  a priori, for instance, based on the knowledge that the employed computer architecture provides  $n_{\text{rand}}$  parallel compute units. In a final step, an SVD of the snapshot matrix is performed to generate the reduced basis according to the prescribed tolerance. This is advantageous in cases where no error estimator is available or an error estimator is very costly to evaluate. As an alternative approach we conjecture that it is possible to develop an adaptive randomized algorithm that adaptively augments the reduced basis relying on a randomized a posteriori error estimator.

**5.3. Choice of probability distribution.** In this subsection we discuss how to choose the probability distribution  $p$  that is used in Algorithm 1 for sampling points in time. In particular, we focus on the following standard sampling methods from randomized NLA [10, 14]: uniform, squared norm, and leverage score sampling. In the following, we first present the probability distributions and subsequently compare them with respect to their approximation properties and computational costs. For an overview on sampling (or column subset selection) techniques, we refer to [10, 14, 21].

Both squared norm and leverage score sampling are non-uniform approaches that incorporate data-dependent information in the construction of the probability distribution. There are possibly two different sources of time-dependent data: variations in the operator  $\mathcal{A}$  (for instance, induced by a diffusion coefficient that varies in time) and source terms and boundary data that are represented by the right-hand side  $\mathcal{F}$ . Depending on the considered problem, one might therefore either sample solely from one of the probability distributions corresponding to  $\mathcal{A}$  or  $\mathcal{F}$  or sample from both distributions simultaneously (cf. subsection 5.3.2).

In the following, we assume that the matrix  $\mathbf{B} \in \mathbb{R}^{N_D \times N_I}$  represents the time-dependent data encoded in  $\mathcal{A}$  or  $\mathcal{F}$ , where  $N_D$  denotes the dimension of the FE space. In case of, for instance, a time-dependent diffusion coefficient, one option is to choose the entries of  $\mathbf{B}$  equal to the value of the diffusion coefficient in the respective space-time nodes. For a time-dependent  $\mathcal{F}$ , one could set the columns of  $\mathbf{B}$  equal to the right-hand side vectors  $\mathbf{F}_l$  for  $0 \leq l \leq N_I - 1$  (cf. (2.3)).

**Uniform sampling.** In the case of uniform sampling, we sample a point of time  $t_i$  with probability  $p_i = 1/N_I$  for  $i = 0, \dots, N_I - 1$ , where  $N_I$  denotes the number of time points determined by the partition  $0 = t_0 \leq \dots \leq t_{N_I-1} = T$  of the time interval  $I$ . The computational costs for constructing the probability distribution are zero.

**Squared norm sampling.** If we employ squared norm sampling [18], we select a point of time  $t_i \in \{t_0, \dots, t_{N_I-1}\}$  with probability  $p_i = \|\mathbf{B}[:, i]\|_2^2 / \|\mathbf{B}\|_F^2$ , where  $\|\cdot\|_F^2$  denotes the Frobenius norm and  $\mathbf{B}[:, i]$  is the  $i$ -th column of  $\mathbf{B}$ . The computation of the probabilities  $p_i$  can be carried out in parallel and its complexity scales linearly in the number of non-zero entries of  $\mathbf{B}$ , e.g. for a dense matrix  $\mathbf{B}$  the computational complexity is  $\mathcal{O}(N_I N_D)$ . The following theorem from [18] gives an additive error bound on the approximation quality of the squared norm sampling approach.

**Theorem 5.5.** ([18, Theorem 2]). *Let  $\mathbf{C} \in \mathbb{R}^{N_D \times c}$  be a sample of  $c$  columns of  $\mathbf{B}$  using the squared norm probability distribution and let  $\mathbf{C}^\dagger$  denote the Moore-Penrose inverse of  $\mathbf{C}$ . Then, with probability at least 0.9 it holds that*

$$(5.2) \quad \|\mathbf{B} - \mathbf{C}\mathbf{C}^\dagger\mathbf{B}\|_F^2 \leq \|\mathbf{B} - \mathbf{B}_r\|_F^2 + \frac{10r}{c} \|\mathbf{B}\|_F^2.$$

Here,  $\mathbf{B}_r$  denotes the best rank- $r$  approximation to  $\mathbf{B}$ .

**Leverage score sampling.** The leverage score sampling approach [15] captures the statistical leverage of the columns of  $\mathbf{B}$  on its best rank- $r$  approximation and preferably chooses columns which have a large influence on the best rank- $r$  fit of  $\mathbf{B}$  [31]. To this end, one computes the leading  $r$  right singular vectors  $\mathbf{v}_1, \dots, \mathbf{v}_r$  of  $\mathbf{B}$  and selects a column  $i$  of  $\mathbf{B}$  (a time point  $t_i \in \{t_0, \dots, t_{N_I-1}\}$ ) with probability  $p_i = 1/r \sum_{j=1}^r \mathbf{v}_j[i]^2$ , where  $\mathbf{v}_j[i]$  is the  $i$ -th entry of  $\mathbf{v}_j$ . The complexity for computing the SVD of  $\mathbf{B}$  is  $\mathcal{O}(r N_I N_D)$ . Alternatively, we can approximate the SVD of  $\mathbf{B}$  via a randomized SVD [21]. The following theorem from [15] gives a multiplicative error bound on the approximation quality of the leverage score sampling approach.

**Theorem 5.6.** ([15, Theorem 3]). *Let  $\varepsilon \in (0, 1]$  and let  $\mathbf{C} \in \mathbb{R}^{N_D \times c}$  be a sample of  $c = 3200 r^2 / \varepsilon^2$  columns of  $\mathbf{B}$  using the leverage score probability distribution. Then, with probability at least 0.7 it holds that*

$$(5.3) \quad \|\mathbf{B} - \mathbf{C}\mathbf{C}^\dagger\mathbf{B}\|_F \leq (1 + \varepsilon) \|\mathbf{B} - \mathbf{B}_r\|_F.$$

Here,  $\mathbf{C}^\dagger$  denotes the Moore-Penrose inverse of  $\mathbf{C}$  and  $\mathbf{B}_r$  denotes the best rank- $r$  approximation to  $\mathbf{B}$ .

**5.3.1. Discussion and comparison of probability distributions.** In the following, we discuss and compare the probability distributions introduced in subsection 5.3 with respect to their approximation properties and computational costs. For a more detailed comparison, we refer to [14].

As no data-dependent information is incorporated, the uniform sampling approach might not detect relevant problem-specific features in time unless a large number of



time points is drawn and can thus lead to poor results. For instance, a data matrix  $\mathbf{B}$  with only one non-zero column would require to draw  $\mathcal{O}(N_I)$  columns (time points) in order to detect the non-zero data at the single point in time with high probability.

Both squared norm and leverage score sampling incorporate information about the data of the problem. In case of squared norm sampling, the probability distribution is based on the values of the matrix as the probability of choosing a column is proportional to its squared Euclidean norm. This perfectly solves the problem of not sampling from columns that are zero. Since leverage scores are based on the (truncated) SVD of  $\mathbf{B}$ , the corresponding probability distribution involves information about the geometry of the subspace spanned by the best rank- $r$  fit of  $\mathbf{B}$ .

Therefore, leverage score sampling can lead to improved approximation results compared to uniform and squared norm sampling as it incorporates knowledge about the underlying geometry of the data encoded in the SVD of  $\mathbf{B}$ . In the numerical experiments we observe that squared norm sampling might not detect parts of the data that have values on smaller scales or smaller temporal scales. In contrast, leverage scores weight the heterogeneous parts of the data equally with the same expectation. As a result, the leverage score sampling approach more likely detects all dominant modes of the heterogeneous data (for more details we refer to [subsection 6.3](#)).

The above observations are in line with the error bounds on the approximation quality of the squared norm and leverage score sampling approach as stated in [Theorems 5.5](#) and [5.6](#). The rank- $r$  best approximation error in [\(5.2\)](#) and [\(5.3\)](#) is given by  $\|\mathbf{B} - \mathbf{B}_r\|_F = (\sum_{i=r+1}^R \sigma_i^2)^{1/2}$  (Eckart-Young theorem e.g. in [\[19\]](#)), where  $\sigma_1 \geq \sigma_2 \geq \dots$  denote the singular values of  $\mathbf{B}$  and  $R \leq \min\{N_D, N_I\}$  denotes its rank. Moreover, the Frobenius-norm in the last term of [\(5.2\)](#) is determined by  $\|\mathbf{B}\|_F = (\sum_{i=1}^R \sigma_i^2)^{1/2}$ . Consequently, error bound [\(5.2\)](#) indicates that in the squared norm sampling approach the number  $c$  of selected columns needs to be large in order to detect structures that correspond to singular values  $\sigma_i$  for which  $\sigma_i/\sigma_j$  with  $i \in \{r+1, \dots, R\}$  and  $j \in \{1, \dots, r\}$  is small. As  $c$  appears in the denominator in the last term of [\(5.2\)](#), it has to be chosen as  $c \approx 10r(\sum_{i=1}^R \sigma_i^2)/(\sum_{i=r+1}^R \sigma_i^2)$  to achieve an error that is of the order of the best rank- $r$  approximation to  $\mathbf{B}$ . In contrast, the bound for the leverage score sampling approach in [\(5.3\)](#) is of the order  $(\sum_{i=r+1}^R \sigma_i^2)^{1/2}$  for a number of selected columns that is independent of the size of the singular values of  $\mathbf{B}$ . However, both error bounds are quite pessimistic and likely overestimate the number of selected columns required for a good quality of approximation.

Nevertheless, the costs for computing the rank- $r$  leverage scores are  $r$  times the costs of computing the squared norm sampling distribution (for a dense matrix  $\mathbf{B}$ ). If the number of time points  $N_I$  and thus the size of the data matrix  $\mathbf{B}$  is large, the computation of the truncated SVD is very costly. To approximate the leading  $r$  right singular vectors, one could employ a randomized SVD and parallelize the computations. This would reduce the computational complexity, but potentially still lead to costs that are not negligible compared to the uniform and squared norm sampling approach.

Consequently, uniform (and squared norm) sampling can be advantageous compared to leverage score sampling if many parallel compute units are available and the data is, for instance, spread over the whole time interval. In that case, one could draw a large number of time points from the uniform (or squared norm) probability distribution and compute all corresponding local solution trajectories employing the computer architecture that allows for many parallel computations. This will likely yield a good



approximation accuracy without having to compute (or approximate) the SVD of a large matrix.

**5.3.2. Sampling from multiple probability distributions.** If both  $\mathcal{A}$  and  $\mathcal{F}$  encode time-dependent data due to, for instance, a diffusion coefficient and source terms that vary in time, one might want to include both data matrices  $\mathbf{B}_{\mathcal{A}}$  and  $\mathbf{B}_{\mathcal{F}}$  in the time point selection process.

To this end, one option is to attach  $\mathbf{B}_{\mathcal{A}}$  to  $\mathbf{B}_{\mathcal{F}}$  and sample from the probability distribution computed from  $[\mathbf{B}_{\mathcal{A}}\mathbf{B}_{\mathcal{F}}] \in \mathbb{R}^{N_D \times 2N_I}$ . However, if the data encoded in  $\mathcal{F}$ , for instance, has values on smaller scales compared to  $\mathcal{A}$  (due to, e.g., high conductivity channels), employing the squared norm sampling approach one might sample solely from the part of the probability distribution that is associated with  $\mathcal{A}$  and neglect the information encoded in  $\mathcal{F}$  (cf. the discussion in [subsection 5.3.1](#)). As leverage score sampling is based on the SVD of  $[\mathbf{B}_{\mathcal{A}}\mathbf{B}_{\mathcal{F}}]$ , the approach more likely detects the dominant modes encoded in both  $\mathcal{A}$  and  $\mathcal{F}$ . Nevertheless, computing the SVD of the large matrix  $[\mathbf{B}_{\mathcal{A}}\mathbf{B}_{\mathcal{F}}] \in \mathbb{R}^{N_D \times 2N_I}$  is more costly than computing the SVDs of  $\mathbf{B}_{\mathcal{A}} \in \mathbb{R}^{N_D \times N_I}$  and  $\mathbf{B}_{\mathcal{F}} \in \mathbb{R}^{N_D \times N_I}$  separately. Therefore, we propose to assemble the probability distributions associated with  $\mathbf{B}_{\mathcal{A}}$  and  $\mathbf{B}_{\mathcal{F}}$  separately and draw from both distributions simultaneously.

## 6. NUMERICAL EXPERIMENTS

In this section we numerically analyze the approximation properties of the reduced basis generated via [Algorithm 1](#). In [subsections 6.1](#) and [6.2](#) we first consider the linear heat equation for time-dependent source terms and comprehensively test how the results depend on various parameters such as the number of chosen time points  $n_{\text{rand}}$ , the local oversampling size  $n_t$ , the number of collected snapshots for the SVD determined via  $k$ , or the probability distribution for drawing points in time. Subsequently, we consider two heterogeneous data sets to further investigate the choice of the probability distribution for drawing time points in [subsection 6.3](#). Finally, we show in [subsection 6.4](#) that the randomized approach is capable of approximating a problem with a time-dependent permeability coefficient that is rough with respect to both space and time using real-world data taken from the SPE10 benchmark problem [\[36\]](#) and demonstrate how to sample from multiple probability distributions simultaneously.

In [subsections 6.1](#), [6.2](#), and [6.4](#) we investigate the linear heat equation as an exemplary model problem of [\(2.1\)](#); see [Remark 4.2](#) for the validation of [Assumption 1](#). For the experiments, we employ the discretization introduced in [section 2](#), use [Algorithm 1](#) to generate the randomized reduced basis, and construct the reduced approximation via Galerkin projection as described in [section 2](#). Moreover, we prescribe homogeneous Dirichlet boundary conditions on  $I \times \Sigma_D$  in all experiments. The complete source code to reproduce all results shown in this section is provided in [\[46\]](#).

**6.1. Stove problem.** In this subsection, we consider the following numerical experiment, which we refer to as Example 1: We choose  $I = (0, 10)$ ,  $D = (0, 1)^2$ ,  $\Sigma_N = \emptyset$ , and discretize the spatial domain  $D$  with a regular quadrilateral mesh with mesh size  $1/100$  in both directions. For the implicit Euler method, we use an equidistant time step size of  $1/30$ . Furthermore, we choose the initial condition  $u_0(x, y) = \sum_{i=1}^3 \sin(i\pi x) \sin(i\pi y)$ , the coefficient  $\kappa \equiv 1$ , and the source term  $f(t, x, y) = \sum_{i=1}^3 f_i(t) f_i(x, y)$  involving three spatially disjoint heat sources (stoves) that are turned on and off in time as illustrated

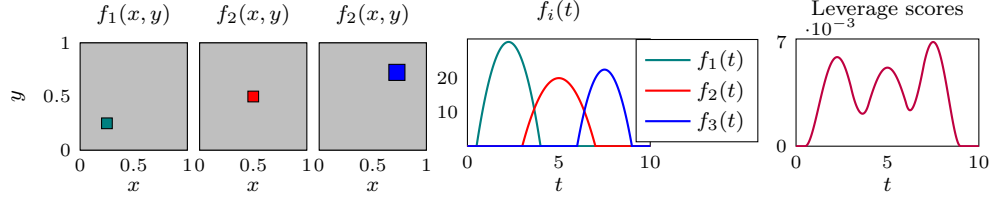


FIGURE 3. Example 1: Source term  $f(t, x, y) = \sum_{i=1}^3 f_i(t) f_i(x, y)$  and corresponding rank-3 leverage score probability distribution. Gray equates to 0, while green, red, and blue equate to 1 (left).

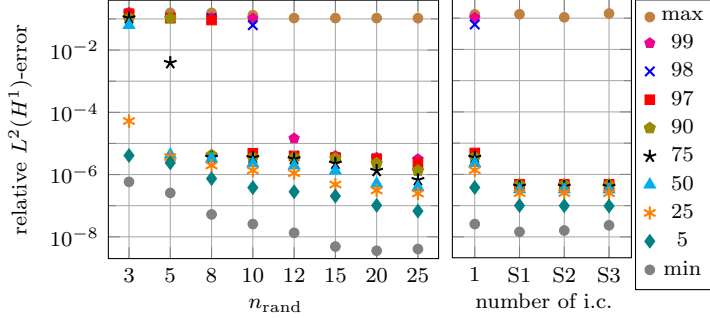


FIGURE 4. Example 1: Quantiles of relative  $L^2(I, H^1(D))$ -error for  $n_t = 15$ ,  $k = 13$ ,  $\text{tol} = 10^{-8}$ , and 100,000 realizations for varying numbers of  $n_{\text{rand}}$  (left) or  $n_{\text{rand}} = 10$  and 1, 2, or 3 random initial conditions (i.c.) per time point (right). Here, S indicates that local computations are performed separately for right-hand side and initial conditions.

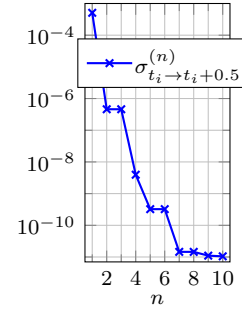


FIGURE 5. Example 1: Singular value decay of transfer operator  $T_{t_i \rightarrow t_i + 15/30}$  ( $0 \leq i \leq 285$ ).

in Fig. 3 (left). Fig. 3 (right) shows the rank-3 leverage score probability distribution computed from the right-hand side matrix  $\mathbf{F}$ , whose columns are the right hand-side vectors  $\mathbf{F}_l$  for  $l = 0, \dots, 300$  (cf. (2.3)). Unless stated otherwise, we use the rank-3 leverage score probability distribution to draw time points in Algorithm 1 for this example.

First, we investigate the influence of the number of drawn time points  $n_{\text{rand}}$  on the approximation accuracy of the reduced basis. As the rank of the right-hand side is three, we choose  $n_{\text{rand}} \geq 3$ . In Fig. 4 (left) we observe that for  $n_{\text{rand}} = 3$  in 50% of cases the error is of the order of  $10^{-1}$  and only in 5% of cases the error is below  $10^{-5}$ , while for  $n_{\text{rand}} = 8$  or  $n_{\text{rand}} = 10$  in 90% or 97% of cases the error is below  $10^{-5}$ . We thus infer that only a small amount of oversampling is necessary to detect all three stoves with high probability. If we choose  $n_{\text{rand}} > 10$  we see in Fig. 4 (left) that the approximation accuracy still slightly improves compared to smaller  $n_{\text{rand}}$ . Nevertheless, we recall that also the computational costs increase with increasing  $n_{\text{rand}}$ . For the following tests in this subsection we therefore choose  $n_{\text{rand}} = 10$  as a good trade-off between approximation accuracy and computational costs.

Next, we test how the approximation accuracy depends on the number of random initial conditions per drawn time point. In Fig. 4 (right) the prefix S indicates that the local solution trajectories are computed separately for right-hand side and homogeneous initial conditions or homogeneous right-hand side and random initial conditions. We observe that for S1-S3 99% of the realizations yield an approximation with a relative  $L^2(I, H^1(D))$ -error below  $10^{-6}$  and the approximation accuracy does not improve if we choose more than one random initial condition. This can be traced back to the

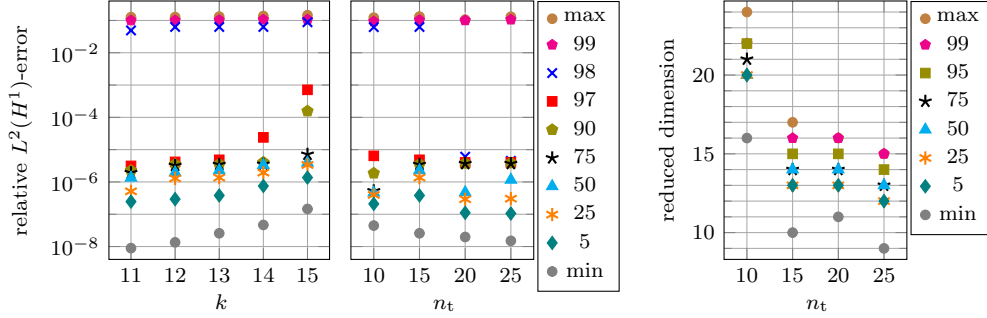


FIGURE 6. Example 1: Quantiles of relative  $L^2(I, H^1(D))$ -error for  $n_t = 15$ , varying numbers of  $k$ ,  $n_{\text{rand}} = 10$ ,  $\text{tol} = 10^{-8}$ , and 100.000 realizations (left). Quantiles of relative  $L^2(I, H^1(D))$ -error (middle) and reduced dimension (right) for varying numbers of  $n_t$ ,  $k = n_t - 2$ ,  $n_{\text{rand}} = 10$ ,  $\text{tol} = 10^{-8}$ , and 100.000 realizations.

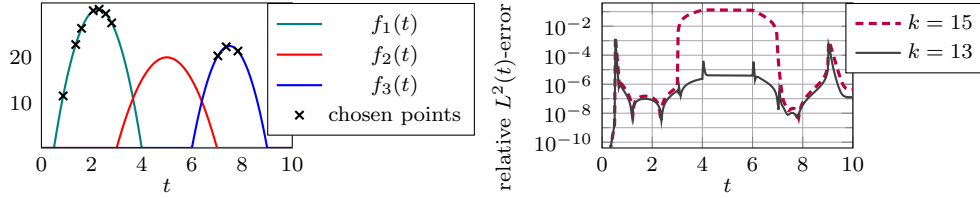


FIGURE 7. Example 1:  $n_{\text{rand}} = 10$  randomly chosen points (left) and relative  $L^2(t)$ -error of corresponding reduced approximation for  $n_t = 15$ ,  $\text{tol} = 10^{-8}$  and  $k = 15$  vs.  $k = 13$  (right).

very fast, exponential decay of the singular values of the transfer operator shown in Fig. 5 (cf. Proposition 5.1). If we draw only one random initial condition per chosen time point and do not separate the local computation for right-hand side and random initial condition, we observe in Fig. 4 (right) that 97% of the realizations yield an approximation with a relative  $L^2(I, H^1(D))$ -error below  $10^{-5}$ . As the approximation accuracy is thus very good and the costs for computing local solutions are only half as much as in the separated approach (S1), we choose to not separate local computations for right-hand side and random initial condition in all other tests in this subsection.

Moreover, we investigate how the number of collected snapshots determined via the parameter  $k$  influences the approximation accuracy of the reduced basis. In Fig. 6 (left) we observe that the approximation quality significantly improves if we collect not only solution snapshots at local end time points ( $k = 15$ ), but at the (locally) last two or three time points ( $k = 14$  or  $k = 13$ ) as, for instance, 75% of realizations have a relative  $L^2(I, H^1(D))$ -error below  $10^{-5}$  for  $k = 15$ , while for  $k = 14$  or  $k = 13$  already 90% or 97% of realizations have a relative  $L^2(I, H^1(D))$ -error below  $10^{-5}$ . Fig. 7 illustrates an explanation for this phenomenon. In the particular realization only time points in the first and last stove are drawn from the probability distribution. However, by choosing  $k = 13$  we include a solution snapshot that also detects the second stove and can thus significantly decrease the error in the time interval (3, 7) for this particular realization compared to  $k = 15$  as shown in Fig. 7 (right). For  $k = 12$  or  $k = 11$  we observe in Fig. 6 (left) only very slight improvements in the approximation quality compared to  $k = 13$ . We therefore choose  $k = n_t - 2$  in all other tests in this subsection as a trade off

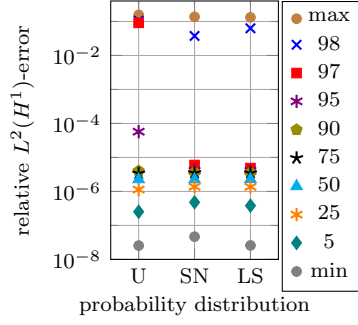


FIGURE 8. Example 1: Quantiles of relative  $L^2(I, H^1(D))$ -error for  $n_{\text{rand}} = 10$ ,  $n_t = 15$ ,  $k = 13$ ,  $\text{tol} = 10^{-8}$ , 100.000 realizations, and uniform (U), squared norm (SN), or leverage score (LS) probability distribution.

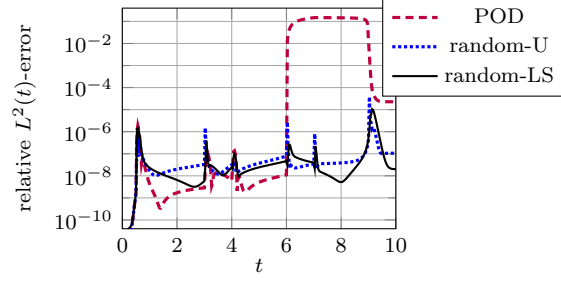


FIGURE 9. Example 1: Relative  $L^2(t)$ -error for one realization of Algorithm 1 for  $n_{\text{rand}} = 10$ ,  $n_t = 15$ ,  $k = 13$ ,  $\text{tol} = 10^{-8}$ , and uniform (random-U) or leverage score (random-LS) probability distribution vs. relative  $L^2(t)$ -error for POD on solution trajectory of first 165 of 300 time steps with tolerance  $10^{-8}$  (POD).

between approximation quality and size of the snapshot matrix and thus computational costs for its SVD.

Subsequently, we test how the approximation accuracy depends on the local oversampling size  $n_t$ , i.e. the number of time steps for which the local solution trajectories are computed. For all tested oversampling sizes, and in particular already for a small oversampling size of  $n_t = 10$ , we observe in Fig. 6 (middle) that 97% of realizations have a relative  $L^2(I, H^1(D))$ -error below  $10^{-5}$  (98% for  $n_t = 20$  and  $n_t = 25$ ). Nevertheless, we see in Fig. 6 (right) that for  $n_t = 10$  the reduced basis is significantly larger compared to  $n_t = 15, 20, 25$  as, for instance, in 95% of cases the reduced dimension is larger than or equal to 20 for  $n_t = 10$ , while for  $n_t = 15, 20, 25$  it is smaller than or equal to 15 in 95% of cases. This can be explained by the fact that for smaller  $n_t$  the randomness of the initial conditions has a larger influence compared to larger  $n_t$  due to the exponential decay behavior of (local) solutions in time. In Fig. 6 (middle) we observe that for  $n_t = 20$  or  $n_t = 25$  the quality of approximation slightly improves compared to  $n_t = 15$ , but we recall that also the computational costs increase with increasing  $n_t$ . For all other tests in this subsection we therefore choose  $n_t = 15$  as a good trade-off between approximation quality, computational costs, and size of the reduced basis.

Next, we investigate how the choice of the probability distribution influences the approximation accuracy for the considered test case. To this end, we employ either the uniform, squared norm, or leverage score probability distribution as introduced in subsection 5.3 for drawing time points in Algorithm 1. Both squared norms and leverage scores are computed from the right-hand side matrix  $\mathbf{F}$ . In Fig. 8 we observe that the squared norm and the leverage score probability distribution yield a comparably good approximation quality and in both cases 97% of realizations have a relative  $L^2(I, H^1(D))$ -error below  $10^{-5}$ . The uniform sampling approach also achieves a good approximation quality as, for instance, 95% (90%) of realizations have a relative  $L^2(I, H^1(D))$ -error below  $10^{-4}$  ( $10^{-5}$ ). Therefore, the results shown in Fig. 8 indicate that for data that is spread over almost the whole time interval, aside from the leverage score sampling approach, the uniform or squared norm sampling approach can also lead to very good approximation results. Especially if the computer architecture allows for

many parallel computations, one can thus save the expenses for computing the SVD of a potentially large data matrix required for the leverage score sampling approach and instead draw a large number of time points from the uniform (or squared norm) probability distribution as discussed in [subsection 5.3.1](#).

As the POD is a well-established tool for compressing and reducing time trajectories, we compare in [Fig. 9](#) the relative  $L^2(t)$ -approximation error for one realization of [Algorithm 1](#) for both the uniform and the leverage score sampling approach with the relative  $L^2(t)$ -error of the approximation via POD on the solution trajectory of the first 165 of 300 time steps. In this way, we compare the standard POD approach with the randomized approach based on the same computational budget of  $(n_{\text{rand}} + 1) \cdot n_t = (10 + 1) \cdot 15 = 165$  time steps. While we also have to compute the SVD of the solution trajectory for the POD and the SVD of the data matrix for the leverage score sampling approach, we here focus on equaling the budget based on the time stepping, which likely dominates the computational costs in complex applications. We observe in [Fig. 9](#) that the POD approach, in contrast to the randomized approach, is not able to detect the third stove due to the reduced computational budget and thus yields a much larger relative approximation error in the time interval  $(6, 9)$  compared to both the uniform and the leverage score sampling approach. Moreover, in the randomized approach the local computations for the initial conditions at  $t = 0$  and the random initial conditions at the 10 randomly chosen time points can be carried out in parallel, while for the POD the 165 time instances of the solution trajectory have to be computed sequentially.

**6.2. Moving stove problem.** Here, we consider the following numerical experiment, which we refer to as Example 2: We choose  $I = (0, 5)$ ,  $D = (0, 1)^2$ ,  $\Sigma_N = \emptyset$ , and discretize the spatial domain  $D$  with a regular quadrilateral mesh with mesh size  $1/100$  in both directions. For the implicit Euler method, we use an equidistant time step size of  $1/30$ . Furthermore, we choose the initial condition  $u_0(x, y) = \sum_{i=1}^3 \sin(i\pi x) \sin(i\pi y)$  and the coefficient  $\kappa \equiv 1$ . As depicted in [Fig. 10](#) (left) we consider a heat source (stove) of size  $0.1 \times 0.1$  that is turned on at  $t = 1$  and moves one degree of freedom in both  $x$ - and  $y$ - direction every three time steps (towards the top right corner of  $D$ ). In total, the stove takes 30 different positions in the spatial domain from time  $t = 1$  to time  $t = 4$  and therefore the rank of the right-hand side is 30. Consequently, the solution of the problem exhibits a heat bubble moving in time and is thus more difficult to approximate compared to the solution of Example 1. For drawing time points in [Algorithm 1](#), we use the rank-30 leverage score probability distribution computed from the right-hand side matrix  $\mathbf{F}$ , whose columns are the right hand-side vectors  $\mathbf{F}_l$  for  $l = 0, \dots, 150$  (cf. [\(2.3\)](#)). In this case, the leverage score probability distribution equals the squared norm probability distribution (cf. [subsection 5.3](#)) and is given by the (scaled) indicator function associated with the time interval  $(1, 4)$ .

As the singular values of the transfer operator for this test case equal the singular values depicted in [Fig. 5](#) and thus decay exponentially fast, we choose to draw only one random initial condition per drawn time point (cf. [subsection 6.1](#)). We investigate how the approximation accuracy is influenced by the number of selected time points  $n_{\text{rand}}$  vs. the number of collected snapshots determined via  $k$ . As the stove moves every three time steps and we choose  $n_t = 15$ , in case of  $k = 13$  we collect solution snapshots at the (locally) last three time instances and thus sample from one stove position in one third of cases and from two stove positions in two thirds of cases. In case of  $k = 11$  we

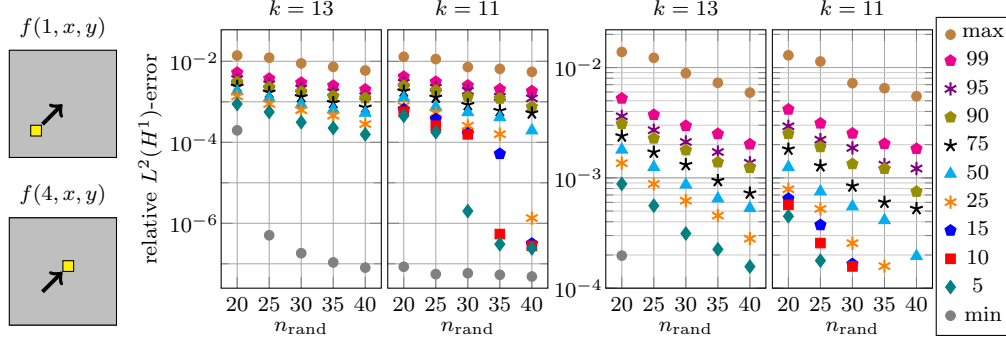


FIGURE 10. Example 2: Source term  $f$  at time  $t = 1$  and  $t = 4$  (left), yellow equates to 10 and gray equates to 0. Quantiles of relative  $L^2(I, H^1(D))$ -error for  $n_t = 15$ ,  $\text{tol} = 10^{-8}$ , 100,000 realizations, varying numbers of  $n_{\text{rand}}$ , and  $k = 13$  vs.  $k = 11$  (right).

collect solution snapshots at the (locally) last five time instances and thus sample from two stove positions in two thirds of cases and from three stove positions in one third of cases.

In order to achieve that in 75% of cases the relative  $L^2(H^1)$  approximation error is below  $10^{-3}$  we observe in Fig. 10 (right) that one needs to choose  $n_{\text{rand}} = 35$  for  $k = 13$  while  $n_{\text{rand}} = 30$  is sufficient for  $k = 11$ . Moreover, for  $n_{\text{rand}} = 25$  (20) we see that 25% (5%) of realizations have a relative  $L^2(H^1)$  approximation error below  $10^{-3}$  in case of  $k = 13$ , while in case of  $k = 11$  this applies for 50% (25%) of realizations. Consequently, the results show that instead of increasing the computational costs by choosing a larger  $n_{\text{rand}}$  one can collect a larger number of already computed snapshots for the SVD to improve the quality of approximation for this test case.

The computational costs of the randomized approach exceed the costs of a standard time trajectory compression (and reduction) via POD for this particular test case. However, we highlight that the computation of the local solution trajectories in Algorithm 1 is embarrassingly parallel while for the POD the global solution trajectory has to be computed in a sequential manner. Depending on the employed computer architecture the randomized approach can thus still lead to a significant speed-up compared to the standard POD approach.

**6.3. Comparison of squared norm and leverage score probability distribution.** In this subsection, we investigate two test cases, which we refer to as Example 3 (a) and (b), for which the squared norm and the leverage score probability distribution differ significantly. We choose  $I = (0, 10)$  and use an equidistant time step size of  $1/30$  for the temporal discretization. The two temporal signals shown in Fig. 11 (a) or (b) correspond to spatially disjoint sources and we compare the squared norm and the rank-2 leverage score probability distribution computed from the right-hand side matrix  $\mathbf{F}$ , whose columns are the right hand-side vectors  $\mathbf{F}_l$  for  $l = 0, \dots, 300$  (cf. (2.3)).

For two signals of the same temporal length but with different values we observe in Fig. 11 (a) that the squared norm approach assigns a much larger probability to the larger than to the smaller signal. In contrast, the leverage score approach assigns the same probability to both signals and weights them equally with expectation 0.5. Moreover, we observe in Fig. 11 (b) for two signals with the same value but of different

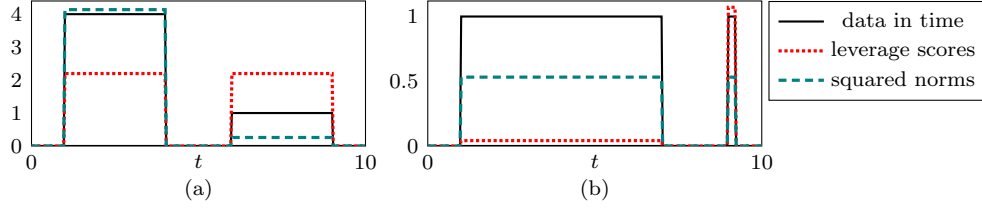


FIGURE 11. Example 3: Rank-2 leverage score (LS) and squared norm (SN) probability distributions for two (spatially disjoint) signals with different values (a) or different temporal scales (b). Values of LS and SN are scaled with a factor of 400 (a) or 15 (LS) and 100 (SN) (b).

temporal length that the squared norm approach assigns the same probability to both signals, while the leverage score approach assigns a much larger probability to the signal of smaller temporal length and again weights the signals equally with expectation 0.5. As already discussed in subsection 5.3.1, this can be explained by the fact that the squared norm probability distribution is computed from the values of  $\mathbf{F}$  while the leverage score sampling approach involves information about the geometry of the data encoded in the SVD of  $\mathbf{F}$ . We can thus expect that the squared norm approach more likely fails to detect the signal of smaller value (a) or smaller temporal length (b) compared to the leverage score approach. Therefore, we conjecture that for data appearing on different scales or different temporal scales the leverage score approach might lead to a better approximation accuracy than the squared norm approach. Moreover, as can be expected from the definition of leverage scores, we observe from numerical experiments not included in this paper that leverage scores are capable of detecting repetitions in the data functions.

**6.4. Problem with a time-dependent permeability coefficient.** In this subsection we consider a numerical experiment including the real-world permeability coefficient  $\kappa_0$  taken from the SPE10 benchmark problem [36], see Fig. 12. We refer to this experiment as Example 4. In Fig. 12 we observe that the solution trajectory of the problem is quite complex due to different configurations and combinations of permeability and inflow into the domain depicted in Fig. 13.

In detail, we choose  $I = (0, 10)$  and  $D = (0, 2.2) \times (0, 0.6)$  with Dirichlet and Neumann boundary as shown in Fig. 13 (left) and discretize the spatial domain  $D$  with a regular quadrilateral mesh with mesh size  $1/100$  in both directions. For the implicit Euler method, we use an equidistant time step size of  $1/50$ . We impose Neumann boundary conditions  $g_N(t, x, y) = g_N(t)$  for  $(x, y) \in (0.4, 1.8) \times \{0.6\}$  modeling a time-dependent inflow as depicted in Fig. 13 (middle) and  $g_N = 0$  elsewhere in  $I \times \Sigma_N$ . The permeability coefficient  $\kappa(t, x, y) = \kappa_0(x, y) + \kappa_1(t) \cdot \kappa_1(x, y) + \kappa_2(t) \cdot \kappa_2(x, y)$  is given by a sum of the permeability field  $\kappa_0$  from [36] shown in Fig. 12 and high conductivity channels  $\kappa_1$  and  $\kappa_2$  that are turned on and off in time as depicted in Fig. 13 (middle). Moreover, the initial conditions are given by  $u_0(x, y) = 1$  for  $(x, y) \in (0.5, 0.7) \times (0.3, 0.4)$  and  $u_0(x, y) = 0$  else. As both the permeability  $\kappa$  and the inflow  $g_N$  vary in time, we sample from two probability distributions simultaneously to draw time points in Algorithm 1 (cf. the discussion in subsection 5.3.2). For this purpose, we employ the rank-3 leverage score probability distribution computed from the matrix, whose columns contain the values of  $\kappa(t_l, \cdot, \cdot)$  for all spatial elements at time point  $t_l$  for  $l = 0, \dots, 500$ . In addition, we use the rank-1 leverage score probability distribution computed from the right



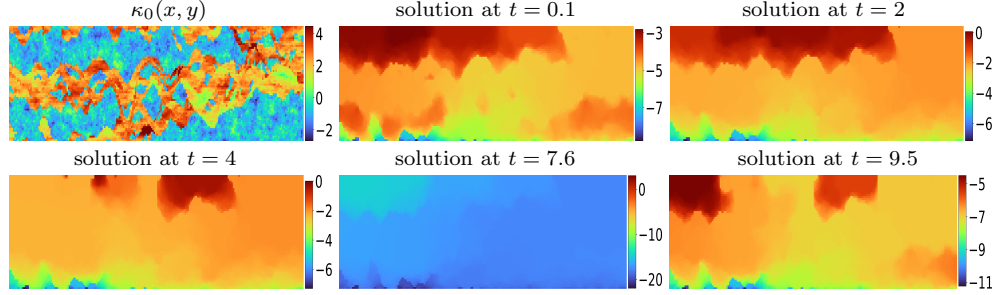


FIGURE 12. Example 4: Permeability field  $\kappa_0$  from [36] and solution evaluated at different points in time, plotted in logarithmic values to the base of 10.

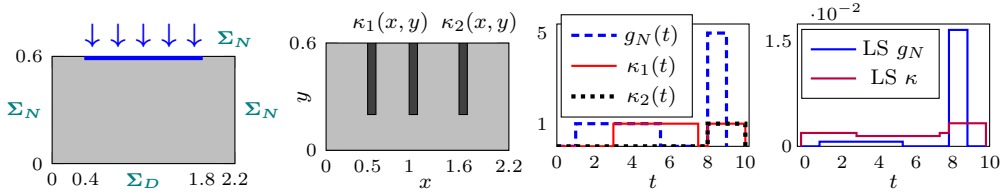


FIGURE 13. Example 4: Dirichlet and Neumann boundary  $\Sigma_D, \Sigma_N$  (left), high conductivity channels  $\kappa_1(t) \cdot \kappa_1(x, y) + \kappa_2(t) \cdot \kappa_2(x, y)$ , and Neumann boundary data  $g_N(t, x, y) = g_N(t)$  for  $(x, y) \in (0.4, 1.8) \times \{0.6\}$ ,  $g_N(t, x, y) = 0$  else (middle). Dark gray equates to  $10^3$ , light gray to 0. Rank-1 leverage scores (LS) associated with  $g_N$  and rank-3 LS corresponding to  $\kappa = \kappa_0 + \kappa_1 + \kappa_2$  (right).

hand-side matrix  $\mathbf{F}$ , whose columns are the right hand-side vectors  $\mathbf{F}_l$  for  $l = 0, \dots, 500$  (cf. (2.3)). Both distributions are depicted in Fig. 12 (right).

First, we test how the approximation accuracy depends on the local oversampling size  $n_t$ . For all tested sizes of  $n_t$ , and especially for a small oversampling size of  $n_t = 10$ , we observe in Fig. 14 (left) that in 88% of cases the relative  $L^2(I, H^1(D))$ -error is below  $2 \cdot 10^{-2}$  and the algorithm succeeds in detecting all different configurations of the time-dependent data functions and thus all different shapes of the solution. Nevertheless, as already observed for Example 1, we see in Fig. 14 (middle) that for  $n_t = 10$  the reduced basis is significantly larger compared to  $n_t = 15$  (20, 25) as, for instance, in 95% of cases the reduced dimension is larger than or equal to 59 for  $n_t = 10$ , while for  $n_t = 15$  (20, 25) it is smaller than or equal to 50 (41, 36) in 95% of cases. The results thus confirm the findings from subsection 6.1 for this test case and in the following we choose  $n_t = 15$  as a good trade-off between approximation quality, computational costs, and size of the reduced basis.

Next, we compare the relative  $L^2(t)$ -approximation error for one realization of Algorithm 1 with the relative  $L^2(t)$ -error of the approximation via POD on the solution trajectory of the first 315 of 500 time steps. As in subsection 6.1, we focus on equaling the computational budget based on the time stepping  $((n_{\text{rand}} + 1) \cdot n_t = (20 + 1) \cdot 15 = 315)$ , which likely dominates the costs in complex applications. In Fig. 14 (right) we observe that the POD yields a much larger error in the time interval (8, 10) compared to the randomized approach and is not able to detect all different configurations of the time-dependent data functions due to the reduced computational budget. Moreover, we emphasize that in the randomized approach the computation of the local solutions can be carried out in parallel, while for the POD the 315 time instances of the global solution trajectory have to be computed sequentially.

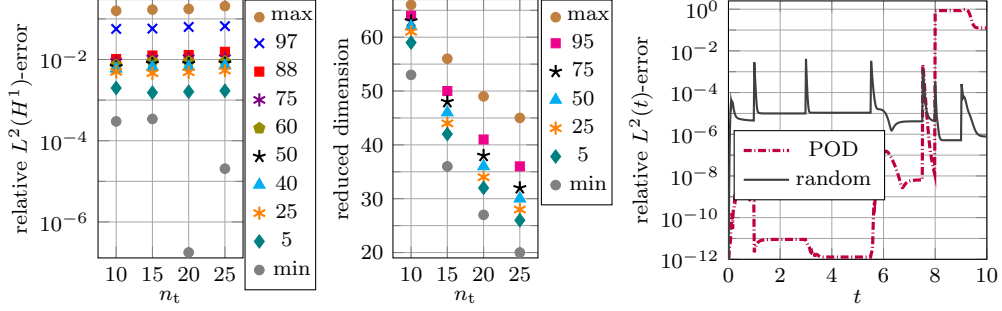


FIGURE 14. Example 4: Quantiles of relative  $L^2(I, H^1(D))$ -error (left) and reduced dimension (middle) for varying numbers of  $n_t$ ,  $k = n_t - 2$ ,  $n_{\text{rand}} = 20(10 + 10)$ ,  $\text{tol} = 10^{-8}$ , and 25,000 realizations. Relative  $L^2(t)$ -error for one realization of Algorithm 1 for  $n_t = 15$  (random) vs. POD on solution trajectory of first 315 of 500 time steps with tolerance  $10^{-8}$  (POD) (right).

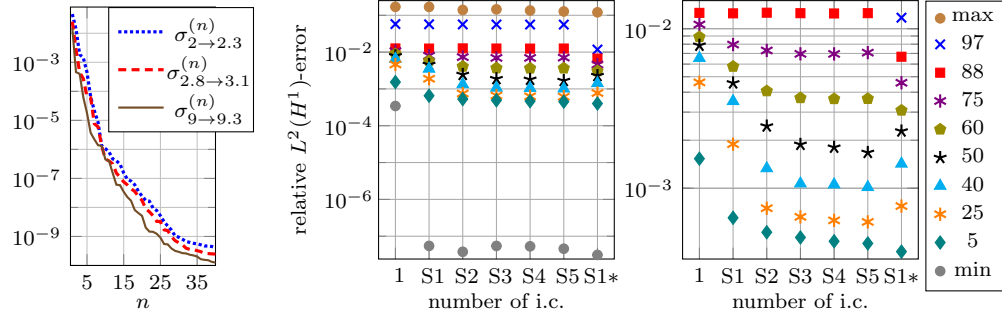


FIGURE 15. Example 4: Singular values of transfer operators (left). Quantiles of relative  $L^2(I, H^1(D))$ -error for  $n_t = 15$ ,  $k = 13$ ,  $n_{\text{rand}} = 20(10 + 10)$ ,  $\text{tol} = 10^{-8}$ , 25,000 realizations, and 1 – 5 random initial conditions (i.c.) per time point (right). S indicates that local computations are performed separately for right-hand side and initial conditions, \* indicates that  $n_{\text{rand}} = 30(15 + 15)$ .

As we observe that the singular values of the transfer operators do not decay as fast as in case of Example 1, see Fig. 15 (left) (and cf. Fig. 5 (right) and the discussion in subsection 6.1), we investigate how the approximation quality depends on the number of random initial conditions per chosen time point. In Fig. 15 (right) we see that the accuracy of the approximation improves if we choose two (S2) instead of one (1, S1) random initial condition per drawn time point. For three or more random initial conditions (S3–S5), the approximation accuracy is at a comparable level with S2. Moreover, we can alternatively improve the approximation quality for this test case by increasing the number of drawn time points  $n_{\text{rand}}$ . If we employ the same computational budget as for S2, but drawn only one random initial condition for 30 instead of 20 drawn time points (S1\*), we observe that in 97% of cases the relative  $L^2(I, H^1(D))$ -error is below  $2 \cdot 10^{-2}$ . Using the same computational budget we thus achieve that the algorithm succeeds to detect all different configurations of the time-dependent data functions in 97% instead of 88% of cases.

## 7. CONCLUSIONS

To tackle time-dependent problems with heterogeneous time-dependent coefficients, we have proposed a randomized algorithm that constructs a reduced approximation

space in time by solving several local problems in time in parallel. Based on techniques from randomized NLA [10, 14, 21] points in time are drawn from a data-driven probability distribution and the PDE is solved locally in time using these points as end points with random initial conditions. The approach allows for local error control [5] and the computation of the local basis functions is embarrassingly parallel.

The numerical experiments demonstrate that the proposed algorithm can outperform the POD even in the sequential setting for complex problems with heterogeneous time-dependent data functions. Moreover, we have observed that leverage scores are capable of detecting multiscale features in the data functions. Based on the experiments we give the following guidance on how to choose the parameters  $n_t$ ,  $k$ , and  $n_{\text{rand}}$ : An appropriate choice for the local oversampling size  $n_t$  is 10 – 15, while for  $n_t = 10$  the resulting reduced basis is larger compared to  $n_{\text{rand}} = 15$ . In addition, we propose  $k = n_t - 2$  as a reasonable choice for diffusion problems, while for advection-dominated problems a smaller  $k$ , for instance,  $k = n_t - 5$ , might be more favorable. The choice of drawn time points  $n_{\text{rand}}$  should be guided by the rank of the time-dependent data functions and can additionally be based on the number of available parallel compute units.

#### APPENDIX A. EXEMPLARY MODEL PROBLEM: THE LINEAR HEAT EQUATION

In this section we consider the linear heat equation as an exemplary model problem of (2.1) and prove both a Caccioppoli inequality and compactness of the corresponding transfer operator. The Caccioppoli inequality is closely linked to the exponential decay behavior of solutions of the PDE in time (cf. the discussion in section 3) and allows to bound the  $L^2(D)$ -norm of solutions evaluated at a point of time in terms of their  $L^2(I, L^2(D))$ -norm. The inequality can thus be used to assess whether the solution space at a point of time is amenable to approximation; facilitating the design of localizable multiscale and model order reduction methods. The combination of a Caccioppoli-type inequality with a suitable compactness theorem is usually used to show compactness of the transfer operator; see also [2, 47, 54, 55].

We seek the temperature  $u : I \times D \rightarrow \mathbb{R}$  such that (cf. also (2.2))

$$\begin{aligned} u_t(t, x) - \operatorname{div}(\kappa(t, x) \nabla u(t, x)) &= f(t, x) && \text{for every } (t, x) \in I \times D, \\ u(t, x) &= 0 && \text{for every } (t, x) \in I \times \partial D, \\ u(0, x) &= u_0(x) && \text{for every } x \in D, \end{aligned}$$

where  $\kappa \in L^\infty(I \times D)^{n \times n}$  denotes the heat conductivity coefficient that satisfies  $\kappa_0(t, x)|v|^2 \leq v^\top \kappa(t, x)v \leq \kappa_1(t, x)|v|^2$  with  $0 < \kappa_0 < \kappa(t, x) < \kappa_1 < \infty$ . Moreover, the heat source and the initial temperature are given by  $f \in L^2(I, H^{-1}(D))$  and  $u_0 \in L^2(D)$ . To simplify notations, we assume homogeneous Dirichlet boundary conditions on  $I \times \partial D$ . However, the theory analogously applies to non-homogeneous Dirichlet (and Neumann) boundary conditions. We may then consider the following weak formulation: Find  $u \in L^\infty(I, L^2(D)) \cap L^2(I, H_0^1(D))$  such that

$$\begin{aligned} - \int_I (u(t), v)_{L^2(D)} \varphi_t(t) dt + \int_I (\kappa(t) \nabla u(t), \nabla v)_{L^2(D)} \varphi(t) dt \\ = \int_I \langle f(t), v \rangle_{H_0^1(D)} \varphi(t) dt \quad \forall v \in H_0^1(D), \varphi \in C_0^\infty(I) \end{aligned}$$

and  $u(0) = u_0$  in  $L^2(D)$ . Here,  $\langle \cdot, \cdot \rangle_{H_0^1(D)}$  denotes the duality pairing between  $H_0^1(D)$  and  $H^{-1}(D)$ . Thanks to the Hahn-Banach theorem we have that

$$u \in W^{1,2,2}(I, H_0^1(D), H^{-1}(D)) := \{v \in L^2(I, H_0^1(D)) \mid v_t \in L^2(I, H^{-1}(D))\}$$

and  $u \in C^0(\bar{I}, L^2(D))$  (see, for instance, [47]). We highlight that the embedding  $W^{1,2,2}(I, H_0^1(D), H^{-1}(D)) \hookrightarrow C^0(\bar{I}, L^2(D))$  is not compact unless additional regularity is assumed. In fact, the generalized Sobolev space

$$W^{1,\infty,r}(I, H_0^1(D), H^{-1}(D)) := \{v \in L^\infty(I, H_0^1(D)) \mid v_t \in L^r(I, H^{-1}(D))\}$$

embeds compactly in  $C^0(\bar{I}, L^2(D))$  for  $r > 1$  [52, Corollary 5]. In contrast, we here prove compactness requiring significantly less regularity. First, the compactness theorem of Aubin-Lions [52, Corollary 5] states that the embedding  $W^{1,2,2}(I, H_0^1(D), H^{-1}(D)) \hookrightarrow L^2(I, L^2(D))$  is compact. Next, the Caccioppoli inequality (cf. [Proposition A.1](#)) is the key ingredient that facilitates the restriction to a point of time as the inequality bounds the  $L^2(D)$ -norm of (local) solutions evaluated at a point of time in terms of their  $L^2(I, L^2(D))$ -norm. Consequently, we prove that the space of (local) solutions contained in the generalized Sobolev space  $W^{1,2,2}(I, H_0^1(D), H^{-1}(D))$  embeds compactly in  $C^0(\bar{I}, L^2(D))$ .

In the following, we denote by  $t^* \in I$  the local end time point to simplify notations in the proofs. We then consider the local time interval  $(s, t^*) \subseteq I$  and seek for local solutions  $u_{\text{loc}} \in L^\infty((s, t^*), L^2(D)) \cap L^2((s, t^*), H_0^1(D))$  with initial conditions  $u_{\text{loc}}(s, \cdot) \in L^2(D)$  such that

$$\begin{aligned} & - \int_s^{t^*} (u_{\text{loc}}(t), v)_{L^2(D)} \varphi_t(t) dt + \int_s^{t^*} (\kappa(t) \nabla u_{\text{loc}}(t), \nabla v)_{L^2(D)} \varphi(t) dt \\ (A.1) \quad & = \int_s^{t^*} \langle f(t), v \rangle_{H_0^1(D)} \varphi(t) dt \quad \forall v \in H_0^1(D), \varphi \in C_0^\infty((s, t^*)). \end{aligned}$$

Employing the compactness theorem of Aubin-Lions [52, Corollary 5], which states that the embedding  $W^{1,2,2}((s, t^*), H_0^1(D), H^{-1}(D)) \hookrightarrow L^2((s, t^*), L^2(D))$  is compact, and the following Caccioppoli inequality we show that the transfer operator  $\mathcal{T}_{s \rightarrow t^*}$  introduced in (4.3) is compact.

**Proposition A.1** (Caccioppoli inequality in time). *Let  $w$  satisfy (A.1) with  $f \equiv 0$  and arbitrary initial conditions  $w(s, \cdot) \in L^2(D)$ . Then, we have that*

$$(A.2) \quad \|w(t^*, \cdot)\|_{L^2(D)}^2 \leq \frac{2}{(t^* - s)} \|w\|_{L^2((s, t^*), L^2(D))}^2 \quad (\text{version 1})$$

or, similarly, for  $q \in (s, t^*)$  we have that

$$\|w(t^*, \cdot)\|_{L^2(D)}^2 + \|\kappa^{1/2} \nabla w\|_{L^2((q, t^*), L^2(D))}^2 \leq \frac{2}{(q - s)} \|w\|_{L^2((s, t^*), L^2(D))}^2 \quad (\text{version 2}).$$

*Proof.* The first paragraph closely follows the proof of Proposition 3.1 in [47]. Since  $w$  satisfies equation (A.1) integration by parts in time yields  $\int_s^{t^*} \langle w_t(t), v \rangle_{H_0^1(D)} \varphi(t) dt + \int_s^{t^*} (\kappa(t) \nabla w(t), \nabla v)_{L^2(D)} \varphi(t) dt = 0$  for all  $v \in H_0^1(D)$  and  $\varphi \in C_0^\infty((s, t^*))$ . As  $\varphi \in C_0^\infty((s, t^*))$  is chosen arbitrarily the fundamental lemma of calculus of variations yields  $\langle w_t(t), v \rangle_{H_0^1(D)} + (\kappa(t) \nabla w(t), \nabla v)_{L^2(D)} = 0$  for all  $v \in H_0^1(D)$  and almost every  $t \in (s, t^*)$ . Next, we introduce a cut-off function  $\eta \in C^1((s, t^*))$  that satisfies  $0 \leq \eta \leq 1$ ,  $\eta(s) = 0$ , and either  $\eta(t^*) = 1$  and  $|\eta_t| \leq \frac{1}{(t^* - s)}$  (version 1) or  $\eta = 1$  in  $(q, t^*)$  and

$|\eta_t| \leq \frac{1}{(q-s)}$  for an arbitrary  $q \in (s, t^*)$  (version 2). In the following, we want to use  $w\eta^2$  as a test function. To enable rearranging the part of the weak formulation that includes the time derivative, we approximate  $w$  by a sequence  $w_n \in C_0^\infty((s, t^*), H_0^1(D))$  such that  $w_n$  converges strongly to  $w$  in  $L^2((s, t^*), H_0^1(D))$ . Then, for almost every  $t \in (s, t^*)$  and each  $n \in \mathbb{N}$  we have that  $\langle w_t(t), w_n(t)\eta^2(t) \rangle_{H_0^1(D)} + (\kappa(t)\nabla w(t), \nabla w_n(t)\eta^2(t))_{L^2(D)} = 0$  and integrating over the time interval  $(s, t^*)$  yields

$$(A.3) \quad \int_s^{t^*} \langle w_t(t), w_n(t)\eta^2(t) \rangle_{H_0^1(D)} dt + \int_s^{t^*} (\kappa(t)\nabla w(t), \nabla w_n(t)\eta^2(t))_{L^2(D)} dt = 0.$$

Using integration by parts twice we can rewrite the first term in (A.3) as follows:

$$\begin{aligned} & \int_s^{t^*} \langle w_t(t), w_n(t)\eta^2(t) \rangle_{H_0^1(D)} dt \\ &= - \int_s^{t^*} (w(t), (w_n(t))_t \eta^2(t))_{L^2(D)} dt - \int_s^{t^*} (w(t), w_n(t) 2\eta(t)\eta_t(t))_{L^2(D)} dt \\ & \quad + (w(t^*), w_n(t^*)\eta^2(t^*))_{L^2(D)} \\ &= - \int_s^{t^*} (w(t)\eta(t), (w_n(t))_t \eta(t))_{L^2(D)} dt - 2 \int_s^{t^*} (w(t)\eta(t), w_n(t)\eta_t(t))_{L^2(D)} dt \\ & \quad + (w(t^*)\eta(t^*), w_n(t^*)\eta(t^*))_{L^2(D)} \\ &= \int_s^{t^*} \langle (w(t)\eta(t))_t, w_n(t)\eta(t) \rangle_{H_0^1(D)} dt - \int_s^{t^*} (w(t)\eta(t), w_n(t)\eta_t(t))_{L^2(D)} dt. \end{aligned}$$

Letting  $n$  go to  $\infty$  thus yields

$$\begin{aligned} & \int_s^{t^*} \langle (w(t)\eta(t))_t, w(t)\eta(t) \rangle_{H_0^1(D)} dt - \int_s^{t^*} (w(t)\eta(t), w(t)\eta_t(t))_{L^2(D)} dt \\ & \quad + \int_s^{t^*} (\kappa(t)\nabla w(t), \nabla w(t)\eta^2(t))_{L^2(D)} dt = 0. \end{aligned}$$

To obtain the final result, we exploit the properties of the cut-off function  $\eta$  and the identity  $\int_s^{t^*} \langle (w(t)\eta(t))_t, w(t)\eta(t) \rangle_{H_0^1(D)} dt = \frac{1}{2} \|w(t^*)\eta(t^*)\|_{L^2(D)}^2$ :

(Version 1) As  $\eta(s) = 0$ ,  $\eta(t^*) = 1$ ,  $0 \leq \eta \leq 1$ , and  $|\eta_t| \leq \frac{1}{(t^*-s)}$ , we infer that

$$\|w(t^*, \cdot)\|_{L^2(D)}^2 \leq \frac{2}{(t^*-s)} \|w\|_{L^2((s, t^*), L^2(D))}^2.$$

(Version 2) As  $\eta(s) = 0$ ,  $\eta = 1$  in  $(q, t^*)$ ,  $0 \leq \eta \leq 1$ , and  $|\eta_t| \leq \frac{1}{(q-s)}$  for  $q \in (s, t^*)$ , we conclude that

$$\|w(t^*, \cdot)\|_{L^2(D)}^2 + \|\kappa^{1/2}\nabla w\|_{L^2((q, t^*), L^2(D))}^2 \leq \frac{2}{(q-s)} \|w\|_{L^2((s, t^*), L^2(D))}^2.$$

□

**Proposition A.2.** *The transfer operator  $\mathcal{T}_{s \rightarrow t^*}$  (cf. (4.3)) is compact.*

*Proof.* Let  $(\xi_n)_{n \in \mathbb{N}}$  be a bounded sequence in  $L^2(D)$ . We denote by  $(w_n)_{n \in \mathbb{N}} \subset L^\infty((s, t^*), L^2(D)) \cap L^2((s, t^*), H_0^1(D))$  the corresponding sequence of solutions of problem (A.1) with initial conditions  $w_n(s) = \xi_n$  in  $L^2(D)$  and right-hand side  $f \equiv 0$ , obtaining  $\|w_n\|_{L^2((s, t^*), H_0^1(D))} \leq c$  for a constant  $0 < c < \infty$ . Then, there exists

a subsequence  $(w_{n_l})_{l \in \mathbb{N}}$  and a limit function  $w \in L^2((s, t^*), H_0^1(D))$  such that the subsequence converges weakly to  $w$  in  $L^2((s, t^*), H_0^1(D))$ . Thanks to this weak convergence we obtain  $-\int_s^{t^*} (w(t), v)_{L^2(D)} \varphi_t(t) dt + \int_s^{t^*} (\kappa(t) \nabla w(t), \nabla v)_{L^2(D)} \varphi(t) dt = 0$ . The Hahn-Banach theorem yields  $w \in W^{1,2,2}((s, t^*), H_0^1(D), H^{-1}(D))$  and thanks to the embedding  $W^{1,2,2}((s, t^*), H_0^1(D), H^{-1}(D)) \hookrightarrow C^0([s, t^*], L^2(D))$  we obtain  $w \in L^\infty((s, t^*), L^2(D))$  and  $w(s, \cdot) \in L^2(D)$ . We may thus infer that  $w$  solves (A.1) with  $f \equiv 0$  and some initial conditions in  $L^2(D)$ . As there also holds that  $(w_{n_l})_{l \in \mathbb{N}} \subseteq W^{1,2,2}((s, t^*), H_0^1(D), H^{-1}(D))$ , the compactness theorem of Aubin-Lions [52, Corollary 5] yields a subsequence  $(w_{n_{l_m}})_{m \in \mathbb{N}}$  which converges strongly to  $w$  in  $L^2((s, t^*), L^2(D))$ . Since the sequence  $e_{n_{l_m}} := w - w_{n_{l_m}}$  thus solves (A.1) with  $f \equiv 0$  and some initial conditions in  $L^2(D)$ , we may invoke version 1 of Proposition A.1 to infer that

$$\|w(t^*, \cdot) - w_{n_{l_m}}(t^*, \cdot)\|_{L^2(D)}^2 = \|e_{n_{l_m}}(t^*, \cdot)\|_{L^2(D)}^2 \leq \frac{2}{(t^* - s)} \|e_{n_{l_m}}\|_{L^2((s, t^*), L^2(D))}^2 \longrightarrow 0.$$

□

#### ACKNOWLEDGMENTS

The authors thank Dr. Alexander Heinlein for providing us with the data file of the permeability field  $\kappa_0$  used in Example 4. Moreover, we thank Dr. Christian Himpe for discussions regarding system and control theory.

#### REFERENCES

- [1] A. ALAOU AND M. W. MAHONEY, *Fast randomized kernel ridge regression with statistical guarantees*, Adv. Neural Inf. Process. Syst., 28 (2015).
- [2] I. BABUŠKA AND R. LIPTON, *Optimal local approximation spaces for generalized finite element methods with application to multiscale problems*, Multiscale Model. Simul., 9 (2011), pp. 373–406.
- [3] G. BERKOOZ, P. HOLMES, AND J. L. LUMLEY, *The proper orthogonal decomposition in the analysis of turbulent flows*, Annu. Rev. Fluid Mech., 25 (1993), pp. 539–575.
- [4] A. BUHR, L. IAPICHINO, M. OHLBERGER, S. RAVE, F. SCHINDLER, AND K. SMETANA., *Localized model reduction for parameterized problems*, in P. Benner, S. Grivet-Talocia, A. Quarteroni, G. Rozza, W.H.A. Schilders, L.M. Sileira (eds.). Model Order Reduction, Volume 2, Snapshot-Based Methods and Algorithms., Walter De Gruyter GmbH, Berlin, 2020.
- [5] A. BUHR AND K. SMETANA, *Randomized Local Model Order Reduction*, SIAM J. Sci. Comput., 40 (2018), pp. A2120–A2151.
- [6] Y. CHAHLAOU AND P. V. DOOREN, *Model reduction of time-varying systems*, in Dimension reduction of large-scale systems, Springer, 2005, pp. 131–148.
- [7] K. CHEN, Q. LI, J. LU, AND S. J. WRIGHT, *Randomized Sampling for Basis Function Construction in Generalized Finite Element Methods*, Multiscale Model. Simul., 18 (2020), pp. 1153–1177.
- [8] E. T. CHUNG, Y. EFENDIEV, W. T. LEUNG, AND S. YE, *Generalized multiscale finite element methods for space-time heterogeneous parabolic equations*, Comput. Math. Appl., 76 (2018), pp. 419–437.
- [9] P. R. CONRAD, M. GIROLAMI, S. SÄRKÄÄ, A. STUART, AND K. ZYGALAKIS, *Statistical analysis of differential equations: introducing probability measures on numerical solutions*, Stat. Comput., 27 (2017), pp. 1065–1082.
- [10] M. DEREZIŃSKI AND M. W. MAHONEY, *Determinantal point processes in randomized numerical linear algebra*, Notices Amer. Math. Soc., 68 (2021), pp. 34–45.
- [11] A. DESHPANDE AND L. RADEMACHER, *Efficient volume sampling for row/column subset selection*, in 2010 IEEE 51st Annual Symposium on Foundations of Computer Science—FOCS 2010, IEEE Computer Soc., Los Alamitos, CA, 2010, pp. 329–338.
- [12] A. DESHPANDE, L. RADEMACHER, S. VEMPALA, AND G. WANG, *Matrix approximation and projective clustering via volume sampling*, Theory Comput., 2 (2006), pp. 225–247.

- [13] P. DRINEAS, M. MAGDON-ISMAIL, M. W. MAHONEY, AND D. P. WOODRUFF, *Fast approximation of matrix coherence and statistical leverage*, J. Mach. Learn. Res., 13 (2012), pp. 3475–3506.
- [14] P. DRINEAS AND M. W. MAHONEY, *RandNLA: Randomized Numerical Linear Algebra*, Commun. ACM, 59 (2016), pp. 80–90.
- [15] P. DRINEAS, M. W. MAHONEY, AND S. MUTHUKRISHNAN, *Relative-error CUR matrix decompositions*, SIAM J. Matrix Anal. Appl., 30 (2008), pp. 844–881.
- [16] J. L. EFTANG AND A. T. PATERA, *Port reduction in parametrized component static condensation: approximation and a posteriori error estimation*, Int. J. Numer. Methods Eng., 96 (2013), pp. 269–302.
- [17] A. ERN AND J.-L. GUERMOND, *Theory and Practice of Finite Elements*, vol. 159 of Applied Mathematical Sciences, Springer New York, New York, NY, 2004.
- [18] A. FRIEZE, R. KANNAN, AND S. VEMPALA, *Fast Monte-Carlo algorithms for finding low-rank approximations*, J. ACM, 51 (2004), pp. 1025–1041.
- [19] G. H. GOLUB AND C. F. VAN LOAN, *Matrix computations*, Johns Hopkins Studies in the Mathematical Sciences, Johns Hopkins University Press, Baltimore, MD, fourth ed., 2013.
- [20] L. GRASEDYCK, I. GREFF, AND S. SAUTER, *The AL basis for the solution of elliptic problems in heterogeneous media*, Multiscale Model. Simul., 10 (2012), pp. 245–258.
- [21] N. HALKO, P. G. MARTINSSON, AND J. A. TROPP, *Finding structure with randomness: probabilistic algorithms for constructing approximate matrix decompositions*, SIAM Rev., 53 (2011), pp. 217–288.
- [22] D. B. P. HUYNH, D. J. KNEZEVIC, AND A. T. PATERA, *A static condensation reduced basis element method: Approximation and a posteriori error estimation*, ESAIM. Math. Model. Numer. Anal., 47 (2013), pp. 213–251.
- [23] L. IAPICHINO, A. QUARTERONI, AND G. ROZZA, *A reduced basis hybrid method for the coupling of parametrized domains represented by fluidic networks*, Comput. Methods Appl. Mech. Eng., 221/222 (2012), pp. 63–82.
- [24] A. KOLMOGOROFF, *Über die beste Annäherung von Funktionen einer gegebenen Funktionenklasse*, Ann. of Math. (2), 37 (1936), pp. 107–110.
- [25] K. KUNISCH AND S. VOLKWEIN, *Galerkin proper orthogonal decomposition methods for parabolic problems*, Numer. Math., 90 (2001), pp. 117–148.
- [26] S. LALL AND C. BECK, *Error-bounds for balanced model-reduction of linear time-varying systems*, IEEE Trans. Automat. Control, 48 (2003), pp. 946–956.
- [27] R. B. LEHOUCQ, D. C. SORENSSEN, AND C. YANG, *ARPACK Users’ Guide*, (1998).
- [28] P. LJUNG, R. MAIER, AND A. MÅLQVIST, *A space-time multiscale method for parabolic problems*, 2021, <https://arxiv.org/abs/2109.06647>.
- [29] C. MA, R. SCHEICHL, AND T. DODWELL, *Novel design and analysis of generalized FE methods based on locally optimal spectral approximations*, 2021, <https://arxiv.org/abs/2103.09545>.
- [30] Y. MADAY AND E. M. RØNQUIST, *A reduced-basis element method*, J. Sci. Comput., 17 (2002), pp. 447–459.
- [31] M. W. MAHONEY AND P. DRINEAS, *CUR matrix decompositions for improved data analysis*, Proc. Natl. Acad. Sci. U.S.A., 106 (2009), pp. 697–702.
- [32] A. MÅLQVIST AND A. PERSSON, *Multiscale techniques for parabolic equations*, Numer. Math., 138 (2018), pp. 191–217.
- [33] A. MÅLQVIST AND D. PETERSEIM, *Localization of elliptic multiscale problems*, Math. Comp., 83 (2014), pp. 2583–2603.
- [34] P.-G. MARTINSSON, V. ROKHLIN, AND M. TYGERT, *A randomized algorithm for the decomposition of matrices*, Appl. Comput. Harmon. Anal., 30 (2011), pp. 47 – 68.
- [35] B. MOORE, *Principal component analysis in linear systems: Controllability, observability, and model reduction*, IEEE Trans. Automat. Contr., 26 (1981), pp. 17–32.
- [36] S. OF PETROLEUM ENGINEERS, *SPE comparative solution project*, <https://www.spe.org/web/csp/datasets/set02.htm>.
- [37] H. OWHADI, *Bayesian numerical homogenization*, Multiscale Model. Simul., 13 (2015), pp. 812–828.
- [38] H. OWHADI AND L. ZHANG, *Localized bases for finite-dimensional homogenization approximations with nonseparated scales and high contrast*, Multiscale Model. Simul., 9 (2011), pp. 1373–1398.



- [39] H. OWHADI AND L. ZHANG, *Gamblets for opening the complexity-bottleneck of implicit schemes for hyperbolic and parabolic ODEs/PDEs with rough coefficients*, J. Comput. Phys., 347 (2017), pp. 99–128.
- [40] H. OWHADI, L. ZHANG, AND L. BERLYAND, *Polyharmonic homogenization, rough polyharmonic splines and sparse super-localization*, ESAIM Math. Model. Numer. Anal., 48 (2014), pp. 517–552.
- [41] A. PINKUS, *n-widths in approximation theory*, vol. 7, Springer-Verlag, Berlin, 1985.
- [42] M. RENARDY AND R. C. ROGERS, *An introduction to partial differential equations*, vol. 13, Springer Science & Business Media, 2004.
- [43] C. W. ROWLEY, *Model reduction for fluids, using balanced proper orthogonal decomposition*, Internat. J. Bifur. Chaos Appl. Sci. Engrg., 15 (2005), pp. 997–1013.
- [44] A. K. SAIBABA, *Randomized discrete empirical interpolation method for nonlinear model reduction*, SIAM J. Sci. Comput., 42 (2020), pp. A1582–A1608.
- [45] H. SANDBERG AND A. RANTZER, *Balanced truncation of linear time-varying systems*, IEEE Trans. Automat. Control, 49 (2004), pp. 217–229.
- [46] J. SCHLEUSS, *Source code to “Randomized quasi-optimal local approximation spaces in time”*, 2022, <https://doi.org/10.5281/zenodo.6287484>.
- [47] J. SCHLEUSS AND K. SMETANA, *Optimal local approximation spaces for parabolic problems*, Multiscale Model. Simul., to appear, (2022+).
- [48] P. J. SCHMID, *Dynamic mode decomposition of numerical and experimental data*, J. Fluid Mech., 656 (2010), pp. 5–28.
- [49] M. SCHOBER, D. K. DUVENAUD, AND P. HENNIG, *Probabilistic ODE solvers with Runge-Kutta means*, Adv. Neural Inf. Process. Syst., 27 (2014).
- [50] M. SCHOBER, S. SÄRKÄ, AND P. HENNIG, *A probabilistic model for the numerical solution of initial value problems*, Stat. Comput., 29 (2019), pp. 99–122.
- [51] S. SHOKOOHI, L. M. SILVERMAN, AND P. M. VAN DOOREN, *Linear time-variable systems: balancing and model reduction*, IEEE Trans. Automat. Control, 28 (1983), pp. 810–822.
- [52] J. SIMON, *Compact sets in the space  $L^p(0, T; B)$* , Ann. Mat. Pura Appl. (4), 146 (1987), pp. 65–96.
- [53] L. SIROVICH, *Turbulence and the dynamics of coherent structures. I. Coherent structures*, Quart. Appl. Math., 45 (1987), pp. 561–571.
- [54] K. SMETANA AND A. T. PATERA, *Optimal local approximation spaces for component-based static condensation procedures*, SIAM J. Sci. Comput., 38 (2016), pp. A3318–A3356.
- [55] T. TADDEI AND A. T. PATERA, *A localization strategy for data assimilation; application to state estimation and parameter estimation*, SIAM J. Sci. Comput., 40 (2018), pp. B611–B636.
- [56] L. TER MAAT, *Random initial conditions in model order reduction*, bachelor thesis, University of Twente, 2019.
- [57] J. H. TU, C. W. ROWLEY, D. M. LUCHTENBURG, S. L. BRUNTON, AND J. N. KUTZ, *On dynamic mode decomposition: Theory and applications*, J. Comput. Dyn., 1 (2014), pp. 391–421.
- [58] B. UNGER AND S. GUGERCIN, *Kolmogorov n-widths for linear dynamical systems*, Adv. Comput. Math., 45 (2019), pp. 2273–2286.
- [59] E. I. VERRIEST AND T. KAILATH, *On generalized balanced realizations*, IEEE Trans. Automat. Control, 28 (1983), pp. 833–844.
- [60] D. P. WOODRUFF, *Sketching as a tool for numerical linear algebra*, Found. Trends Theor. Comput. Sci., 10 (2014), pp. iv+157.

FACULTY OF MATHEMATICS AND COMPUTER SCIENCE, UNIVERSITY OF MÜNSTER, EINSTEINSTR. 62, 48149 MÜNSTER, GERMANY, JULIA.SCHLEUSS@UNI-MUENSTER.DE.

DEPARTMENT OF MATHEMATICAL SCIENCES, STEVENS INSTITUTE OF TECHNOLOGY, 1 CASTLE POINT TERRACE, HOBOKEN, NJ 07030, UNITED STATES OF AMERICA, KSMETANA@STEVENS.EDU.

CURRENTLY MASTER STUDENT AT THE UNIVERSITY OF TWENTE, THE NETHERLANDS, PRIVATE ADDRESS: KIEFTSBEEKLAAN 33, 7607TA ALMELO, THE NETHERLANDS, LUKAS.TM@HOTMAIL.NL.